Laboratori Nazionali di Frascati

LNF-92/090 (P)
4 Novembre 1992

J.L. Franzini, W. Kim, P.J. Franzini:

STUDYING THE F_0 AND η' AT DAΦNE

Contribution to the DAΦNE Physics Handbook

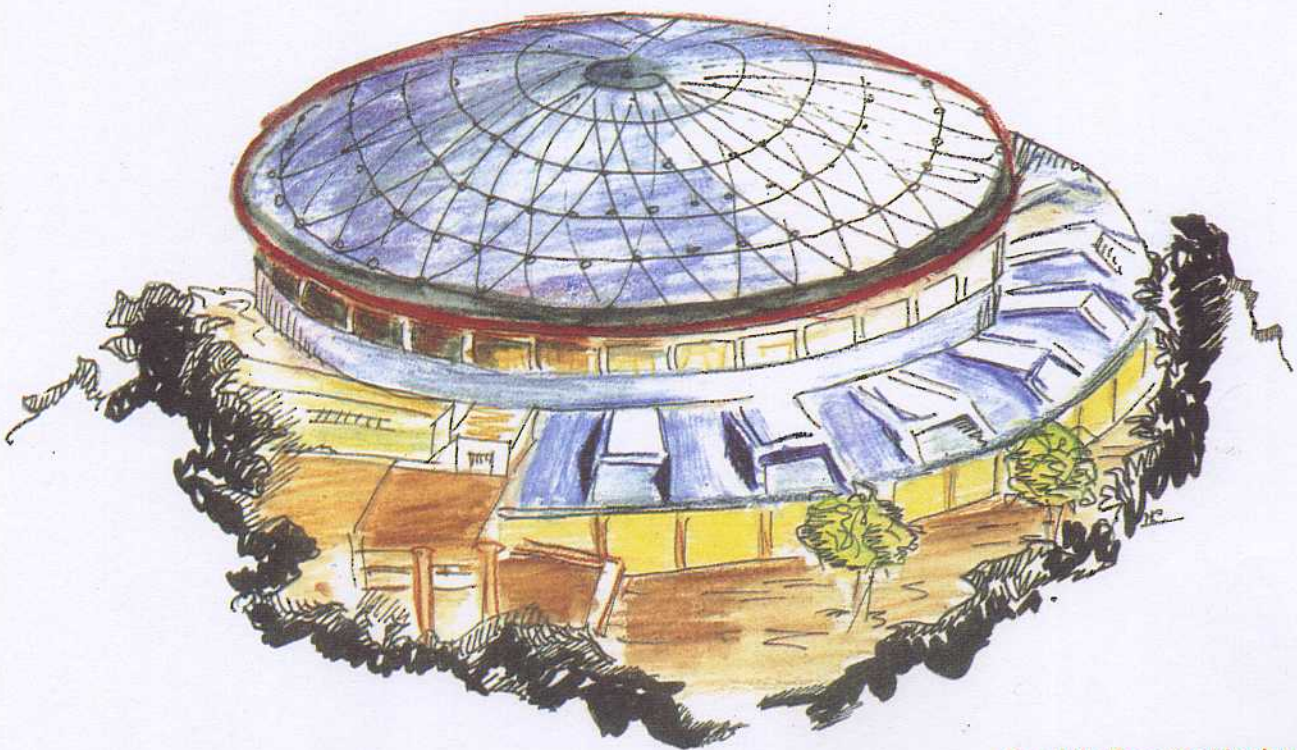

Servizio Documentazione
dei Laboratori Nazionali di Frascati
P.O. Box, 13 - 00044 Frascati (Italy)

INFN - Laboratori Nazionali di Frascati
Servizio Documentazione

LNF-92/090 (P)
4 Novembre 1992

STUDYING the f_0 and η' at DAΦNE

JULIET LEE-FRANZINI

Laboratori Nazionali di Frascati dell'INFN

SUNY at Stony Brook, Stony Brook, New York 11794

WON KIM

SUNY at Stony Brook, Stony Brook, New York 11794

PAULA J. FRANZINI

Laboratoire de Physique Théorique ENSLAPP,[⋆]
B.P. 110, F-74941 Annecy-Le-Vieux Cedex, France

Abstract

At the end of 1995, the Frascati ϕ–factory will begin delivering of the order of 500 ϕ-mesons/sec. This provides a unique opportunity to study the $f_0(975)$ in ϕ radiative decays, even for branching ratios which in some estimates could be as low as 1×10^{-6}. This unique, lightest scalar meson state is poorly described by current models, and more information is essential. By Monte Carlo studies we show that the smallest expected branching ratio can easily be measured in the decay $f_0\to\pi^0\pi^0$. In decays to $\pi^+\pi^-$, there are backgrounds from continuum processes. Interference between one of these processes and the f_0 amplitude leads to very interesting and complex patterns. A complete study of the photon spectrum from $e^+e^-\to\pi^+\pi^-\gamma$ at the ϕ peak, after suppression of continuum contributions by suitable kinematics and angular cuts, can determine the sign of the $\phi f_0\gamma$ coupling even for the smallest branching ratio, thus providing a totally new piece of information for the investigation of the nature of the f_0. A similar study of the decay $\phi\to\eta'\gamma$ shows that its branching ratio can be measured with very good accuracy, therefore measuring the gluon contents of light pseudoscalar mesons to high accuracy.

⋆ *URA 14-36 du CNRS, associée à l'E.N.S. de Lyon, et au L.A.P.P. d'Annecy-le-Vieux*

1. INTRODUCTION

DAΦNE,[1] beginning in 1995, will deliver a luminosity $\mathcal{L}\sim10^{32}$ cm^{-2} s^{-1}, yielding of the order of 5 billion ϕ's in four months of machine-on time: $5[\mu b]\times10^{32}[cm^{-2}\ s^{-1}]\times10^{7}$ [s]$=5\times10^{9}$. In the following we assume that 5×10^{9} ϕ mesons are collected in the first year, while DAΦNE is tuned to reach maximum $\mathcal{L}$. This constitutes an enormously large sample of ϕ's, previously unavailable, and gives the possibility of detecting rare ϕ decays, especially rare radiative decays which typically are predicted to have branching ratio's (BR) of the order of 10^{-4} to 10^{-7}.[2] Existing experimental measurements are few. The most common radiative mode is $\phi\to\eta^0\gamma$ with BR($\phi\to\eta^0\gamma$)$=0.0128\pm0.0006$; the next most frequent mode $\phi\to\pi^0\gamma$ is measured to an accuracy of only 30%: BR($\phi\to\pi^0\gamma$)$=(0.31\pm0.13)\times10^{-3}$.[3] Many modes which are not forbidden by symmetry arguments, but are very interesting from a spectroscopic point of view, such as $\phi\to\eta'\gamma$, $\to f_0\gamma$, $\to a_0\gamma$, $\to\pi^+\pi^-\gamma$, $\to\pi^0\pi^0\gamma$, $\to\pi^0\eta\gamma$, have not been observed at all and upper limits of the order of 10^{-3} are given. About the C violating decays $\phi\to\omega\gamma$, $\to\rho\gamma$, $\to\eta\pi^0$ we know nothing; upper limits are of the order of 10^{-2}.[3] We discuss in the following detector issues associated with measuring rare radiative decays amidst prolific background events arising from $\phi\to X+\pi^0(\to 2\gamma)$ decays, with specific examples: $\phi\to f_0\gamma$ and $\phi\to\eta'\gamma$. We show that background processes, though they might be much larger than the signal, can be well controlled by appropriate kinematical cuts.

For the case of $f_0\to\pi^+\pi^-$, additional backgrounds come from continuum processes such as coupling of the initial e^+e^- state to the tail of the ρ, an *initial state radiation process*, and $e^+e^-\to\mu^+\mu^-\gamma$ if muons are mistaken for pions. Furthermore, the ϕ can produce a pair of pions through off-shell ρ production with one of the pions radiating a γ, a *final state radiation process*. We shall call $A_{\rho^\bullet}$ the amplitude for this process and A_{f_0} the amplitude for $\phi\to f_0\gamma\to\pi^+\pi^-\gamma$.

While initial state radiation only contributes an incoherent background, as it is the only $\phi\to\pi\pi\gamma$ process antisymmetric under pion exchange (C($\pi^+\pi^-$)=-1), the amplitudes $A_{\rho^\bullet}$ and A_{f_0} do interfere, because the pions from ρ decay with final state radiation are in a C–even state, as are those from f_0 decay.[4,5] The sign of the interference term is unknown, since it depends on the sign of the $\phi f_0\gamma$ coupling and therefore on the unknown nature of the f_0.[2] While the magnitude of final state radiation is approximately one tenth of that for initial state radiation, the f_0 signal is comparable or smaller than the former, by as much as a factor of ten to one hundred. The interference term can drastically alter the f_0 signal in ϕ decays, both in shape and in magnitude. For the

case of destructive interference, the f_0 signal can become woefully small, indeed, was expected to essentially disappear in Ref. 5. However, since the shape of the interference term and its angular distributions are different from those from $|A_{f_0}|^2$, the presence of an f_0 signal can always be recognized, even when cancellation is maximal. We only lose sensitivity to the presence of f_0's in ϕ decays when the branching ratio for $\phi \to f_0\gamma$ ($\mathrm{BR}_{\phi f_0\gamma}$) becomes smaller than about 3×10^{-7}. In addition, the shape of the signal allows in general to determine the sign of the interference term and therefore of the $\phi\to f_0\gamma$ amplitude, another valuable piece of information about the poorly-understood f_0. The $\mu^+\mu^-\gamma$ background, while much larger than the signal, can be easily removed in a detector such as KLOE,[6] by appropriate kinematical cuts. The initial state radiation contribution can be strongly suppressed by angular cuts. Thus we find the conclusions of ref. 5 more pessimistic than necessary.

2. SPECTROSCOPY DETECTORS

2.1 Precision EM Calorimeters

Spectroscopy requiring detection of neutral particles in the final state has been done in the more recent past with dedicated electromagnetic calorimeters, often composed of scintillating crystals (NaI, BGO, CsI), which give excellent photon energy resolution. Typically a minimal level of tracking with no magnetic field is provided, thus there is no momentum determination for charged particles. This allows to distinguish between charged and neutral particles, and gives the direction of charged particles and the entry point of tracks into the calorimeter. To reconstruct the neutral particles (π^0, η etc.), whose decay products include photons, it is necessary to determine the direction of the final state photons. This is obtained by segmenting the calorimeter into many polar and azimuthal elements to find the electromagnetic (EM) shower centroid to the required accuracy. With highly segmented calorimeters, particle identification is accomplished by recognizing the characteristic energy deposition patterns of particles in the crystals. EM showers from an electron or photon have typical longitudinal and transverse profiles which allow rejection of spurious signals to the 10^{-2} - 10^{-3} level. Minimum ionizing particles have constant energy deposition along their paths. Strongly interacting particles, hadrons, may undergo nuclear interactions in the crystals, exhibiting a discontinuous energy deposition pattern at the point of interaction. If the calorimeter is longitudinally segmented finely enough, particle identification can also be aided by

range measurements. The most crucial considerations in obtaining the ideal energy resolution from these calorimeters is to have

1. constant monitoring of the crystal to crystal calibrations, and
2. a precise overall energy scale determination.

The implementation of a neutral particle spectrometer at one of DAΦNE's interaction regions is highly desirable because

1. the luminosity required for spectroscopy studies is less than that required for CP violation studies,
2. neutral particle calorimeters are compact and easier to install and become operational, especially if one transports to DAΦNE a proven world-class spectrometer which can be recycled at the time of DAΦNE's commissioning.

We chose the CUSB-II Spectrometer[7] for our Monte Carlo (MC) feasibility studies of measuring rare radiative ϕ decays at DAΦNE with a neutral particle spectrometer. After the completion of upsilon spectroscopy studies at CESR for a decade, CUSB has been disassembled, packed in crates, stored *in toto* at the Nevis Laboratories and is available for being reassembled at DAΦNE if needed.

2.2 General Purpose Detectors

These detectors consist of large tracking devices in magnetic field and EM calorimeters inside or outside the coil producing the field. They can measure energy or momenta of charged and neutral particles as well, usually with lower precision for photons, but compensate for this by more complete sensitivity to the full event topology and kinematics. We will also quote in a following section the results of an incomplete MC study of the sensitivity to rare radiative ϕ decay of an operating magnetic spectrometer, the CMD2.[8] This spectrometer has its EM calorimeter outside the magnetic coil, resulting in poor energy resolution for low energy photons.

The majority of our results come from simulations in the KLOE detector.[6] The detector, surrounding a thin, 10 cm radius beam pipe, consists of a drift chamber with a helium-based gas mixture, of 2 m radius and 4 m length, providing a momentum resolution of ~0.45%, at the range of interest. The chamber is surrounded by a hermetic (solid angle coverage greater than 98%) electromagnetic calorimeter with three-dimensional readout. The EM calorimeter consists of sandwiches of very thin (0.5mm), grooved, lead foils and 1 mm diameter scintillating fibers. Its energy resolution is $5\%/\sqrt{(E/1\mathrm{GeV})}$,

with full efficiency for 20 MeV photons, and has exceptional timing performance, 300 ps/$\sqrt{(E/20\text{MeV})}$. The angular reslution for photons is excellent, $\sim\pm5$ mrad.

3. $\phi\rightarrow f_0\gamma$

3.1 $f_0\rightarrow\pi^0\pi^0$

We chose for our MC studies the reaction $\phi\rightarrow f_0\gamma$, where the f_0 decays into a $\pi^+\pi^-$ pair or into two π^0's. The branching ratio for this reaction is interesting because of:

1. the implications it has for the measurement of $\Re(\epsilon'/\epsilon)$ and$\Im(\epsilon'/\epsilon)$,
2. the value it has in its own right from a spectroscopic point of view. See the discussion of Brown and Close.[2]

This decay has not been observed yet. The experimental limit is of the order of 2×10^{-3}, which is much higher than the most optimistic theoretical expectation of 2.5×10^{-4}.[9] Partial wave analysis suggests that 78% of the f_0's decay to two pions (1/3 neutral, 2/3 charged), 22% to a pair of K's.

The signature for the decay $\phi\rightarrow f_0\gamma$, $f_0\rightarrow\pi^0\pi^0$ is five photons, with one of the photons having $\sim$50 MeV and four of the photons reconstructing to a pair of nearly collinear π^0's, whose invariant mass sums up to that of the f_0. The possible background events are from:

1. $\phi\rightarrow\pi^0\pi^0\gamma$, experimentally not yet detected, with an upper limit of BR$<1\times10^{-3}$. Measured values in this paper are taken from the Particle Data Book[3] unless otherwise specified. Predicted values for this process via a virtual ρ vary from 1.2×10^{-5},[10,11] to 3.62×10^{-5}.[12]
2. $\phi\rightarrow\pi^0\rho^0$ with $\rho\rightarrow\pi^0\gamma$. The product branching ratio of these two observed processes is BR$=(3.4\pm0.88)\times10^{-5}$.
3. $\phi\rightarrow\pi^0\rho^0$ with $\rho\rightarrow\eta\gamma$, $\eta\rightarrow2\gamma$, with the product BR from the three observed processes, BR$=(6.4\pm1.2)\times10^{-6}$, all of which yield five photons.
4. $\phi\rightarrow\gamma\eta$ with $\eta\rightarrow3\pi^0$, with product BR from the observed two processes: BR $=(4.1\pm2.0)\times10^{-3}$, and two of the photons are not detected in the calorimeter.

There is no background arising from $\phi\rightarrow K_SK_L$ where the K_S decays into $2\pi^0$'s and the K_L decays into $3\pi^0$'s and five photons are missed. The (acceptance$\times K_L$ decay probability)$\times$BR, $\mathcal{A}$, in CUSB is 5.8×10^{-5}, in KLOE 3.1×10^{-10}. This is before applying any energy-momentum constraint.

To be on the conservative side, we have considered background (1) both at the estimated level found theoretically in Refs. 10 and 11, and at the much larger level allowed by the current experimental bound. We have treated background (2) separately from background (1) because it can be best dealt with experimentally using the constraint of a physical ρ. Moreover, we suspect that the theoretical estimate of background (1) in Refs. 10 and 11 might be low by a factor of two or three since the estimates in the same model for the $\phi \to \pi^0\rho^0$ and $\rho \to \pi^0\gamma$ branching ratios are also low. $\phi \to \pi\rho \to \pi\eta\gamma$ can also be treated similarly as background (1). If we use the theoretical estimate via a virtual ρ,[11] (3) is negligible; if we use the experimental value, it is a similar exercise to that of considering background (1).

Using the CUSB Monte Carlo program, signal and background processes were generated and the particles followed through in the CUSB spectrometer. For the $\phi \to \pi^0\pi^0\gamma$ process we have used the matrix elements with angular distributions from reference 10. For completeness of the DAΦNE Physics Handbook, we include them in this paper in the appendix. Photon spectra and acceptance×detection efficiencies (ϵ) for each process were obtained after applying the following selection criteria: five and only five photons are present in the detector; four of the photons are paired into two π^0's whose reconstructed mass must be within 50 MeV of the π^0 mass; the reconstructed f_0 mass from the two pions must be within 50 MeV of the expected mass peak at 975 MeV; the energy of the leftover photon is to be less than 95 MeV, and, finally, the invariant mass of all the decay products must be within 50 MeV of the known ϕ mass. ϵ for the signal in CUSB is $(9.7\pm0.1)\times10^{-2}$. This small CUSB value arises from the fact that CUSB central calorimeter covers a solid angle of $0.7\times4\pi$, which results in a geometrical acceptance for five photons of 0.17 (to be contrasted with KLOE which covers over 98% of 4π, thus resulting in a geometrical acceptance for five photons of 0.92). The application of kinematical cuts, reconstruction of pions, and f_0, etc., account for the rest of the loss. CUSB has superb photon energy resolution, which is given by $\sigma(E_\gamma)/E_\gamma = 2\%/\sqrt[4]{E_\gamma}$ where E_γ is measured in GeV. The compensation for applying all the selection criteria in CUSB is that the ϵ's for backgrounds 1–3 are down by about a factor of 42, and, background (4) is negligible. Table Ia summarizes the experimental numbers.

Table Ia. BR and ϵ for neutral final states in CUSB and KLOE

PROCESS	BR	ϵ_{CUSB}	ϵ_{KLOE}
$\phi \to f_0+\gamma \to \pi^0\pi^0+\gamma$	$(0.26\text{–}65)\times10^{-6}$	9.7×10^{-2}	8.4×10^{-1}
$\phi \to \pi^0\pi^0\gamma$	$(1.2\text{–}100)\times10^{-5}$	1.5×10^{-4}	1.3×10^{-3}
$\phi \to \pi^0+\rho^0 \to \pi^0+\pi^0\gamma$	3.4×10^{-5}	4.4×10^{-3}	8.4×10^{-4}
$\phi \to \pi^0+\rho^0 \to \pi^0+\eta\gamma$	6.4×10^{-6}	1.0×10^{-3}	8.4×10^{-4}
$\phi \to \gamma+\eta \to 3\pi^0+\gamma$	4.1×10^{-3}	1.5×10^{-7}	$<1\times10^{-7}$

All spectra of background photon surviving the cuts were fitted to polynomials, $g(k)$ where k is the photon energy. The signal can be fitted to a Breit-Wigner form, $s(k)$. Using the *a priori* error estimate,[13] the fractional accuracy of the signal BR is given by:

$$\frac{\delta(\mathrm{BR})}{\mathrm{BR}} = \frac{1}{\mathrm{BR}}\frac{1}{\sqrt{N}}\Big(\int \frac{1}{f(k)}\Big(\frac{\partial f(k;\mathrm{BR})}{\partial \mathrm{BR}}\Big)^2 \mathrm{d}k\Big)^{-\frac{1}{2}} \tag{3.1}$$

where

$$f(k) = \sum_1^4 \epsilon_{bcknd,i} \times \mathrm{BR}_{bcknd,i} \times g_i(k) + \epsilon_{signal} \times \mathrm{BR}_{signal} \times s(k).$$

Thus, in a year's run at DAΦNE ($\sim5\times10^9$ ϕ's), CUSB can measure BR($\phi \to f_0\gamma$) using the two $\pi^0\pi^0$ decay mode, from 0.4% to 14% accuracy over the expected range of theoretical predictions if the BR for direct $\phi \to \pi^0\pi^0\gamma$ is the one expected theoretically. If the direct $\phi \to \pi^0\pi^0\gamma$ BR is at the experimental limit the smallest $\mathrm{BR}_{\phi f_0\gamma}$ that CUSB can measure to 5 sigma accuracy is 1.0×10^{-6}, which means that any good spectrometer can access the smallest branching ratio. These results are tabulated in Table Ib.

Applying the same selection criteria in KLOE, the loss in signal is much less severe, because for this particular decay involving five photons from a wide parent signal (f_0) peak, it is more important for kinematical fitting and reconstruction to have small photon losses than extremely precise energy resolution.

The efficiencies in KLOE for the f_0's neutral decay mode is estimated to be 84%, 30 times better than CUSB.[14] The accuracy attainable by KLOE in the same corresponding period is shown in the last column of table Ib. One expects superb sensitivities to the signal over the whole range of signal and background BR's examined.

Table Ib. Fractional error in BR($\phi \rightarrow f_0\gamma$) for CUSB and KLOE

BR($\phi \rightarrow f_0\gamma$)	BR($\phi \rightarrow \pi^0\pi^0\gamma$)	δ(BR)/BR CUSB	δ(BR)/BR KLOE
1.0×10^{-6}	1.2×10^{-5}	0.140	0.025
2.5×10^{-4}	1.2×10^{-5}	0.004	0.002
1.0×10^{-6}	1.0×10^{-3}	0.180	0.044
2.5×10^{-4}	1.0×10^{-3}	0.005	0.0015

Fig. 1 shows the photon spectrum in CUSB from one year's run with BR($\phi \rightarrow f_0\gamma$) = 2.5×10^{-4} and BR($\phi \rightarrow \pi^0\pi^0\gamma$)= 1×10^{-3}.

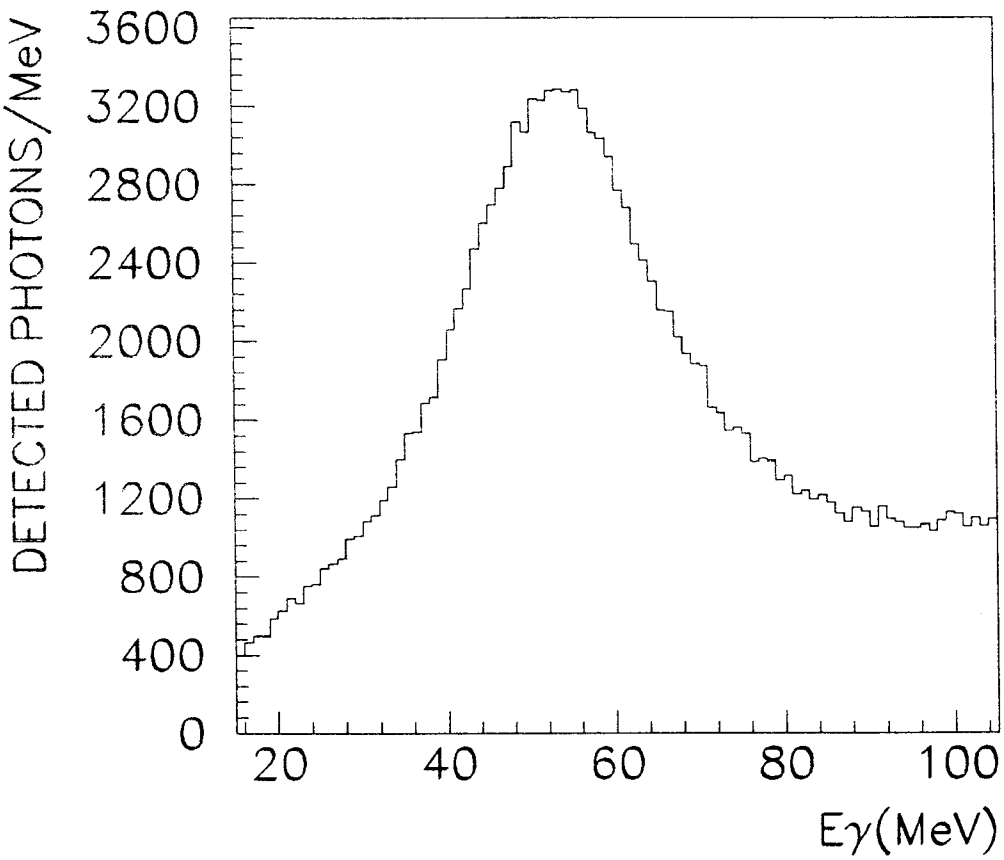

Figure 1. Photon Spectrum (Signal + Background) in CUSB from $\phi \rightarrow f_0\gamma$.

3.2 $f_0 \rightarrow \pi^+\pi^-$

3.2.1 Backgrounds from misidentified ϕ decays

The signature for $\phi \rightarrow f_0\gamma$, $f_0 \rightarrow \pi^+\pi^-$ is a pair of nearly collinear charged pions, whose invariant mass equals that of the f_0, and one low energy photon. The possible

backgrounds from misidentified ϕ decays are

1. $\phi \to \pi^+\pi^-\pi^0$, BR=$(1.9\pm1.1)\times10^{-2}$.
2. $\phi \to \pi^0\rho^0 \to \pi^0\pi^+\pi^-$, product BR= $(4.3\pm0.2)\times10^{-2}$.
3. $\phi \to \pi^\pm\rho^\mp \to \pi^0\pi^+\pi^-$, product BR=$(8.6\pm0.5)\times10^{-2}$.

These reactions yield two oppositely charged pions and one neutral pion, so contribute to the background if one photon is not detected.

There is no background arising from $\phi \to K_S K_L$ where the $K_S \to \pi^+\pi^-$and $K_L \to 3\pi^0$'s and five photons are not detected. $\mathcal{A}$ for CUSB is of the order of 1.2×10^{-5}, and for KLOE it is 1.7×10^{-11}. Nor is there from $\phi \to K_S K_L$ where $K_S \to \pi^0\pi^0$ and $K_L \to \pi^+\pi^-\pi^0$ or $\pi^\pm\mu^\mp\nu$, and five or three photons are undetected. $\mathcal{A}$ for CUSB is of the order of 3.3×10^{-6} and 5.3×10^{-5} for the two processes; for KLOE the corresponding $\mathcal{A}$'s are 4.5×10^{-12} and 5.4×10^{-8}. Finally, there is also no background arising from $\phi \to K_S K_L$ where the $K_S \to \pi^+\pi^-$and $K_L \to \gamma\gamma$ and one photon is not detected. $\mathcal{A}$ for CUSB is of the order of 1.4×10^{-6}, for KLOE 1×10^{-6}. All these numbers are obtained before applying the energy-momentum conservation constraint.

Again, signal and background processes were simulated in the CUSB spectrometer. We used the following selection criteria: two tracks and one photon are present in the detector; the opening angle between the two tracks is within 2° of 175°; the energy of the photon is within 10 MeV of 53 MeV. Table IIa summarizes the BR's and ϵ's for the background processes and the signal, for the three detectors. Table IIb gives the fractional error in measuring the signal BR, calculated as in the previous section.

Table IIa. BR and ϵ for $\pi^+\pi^-\gamma$: $\phi \to f_0\gamma$ signal and backgrounds with one lost γ

PROCESS	BR	$\epsilon(CUSB)$	$\epsilon(KLOE)$
$\phi \to f_0\gamma \to \pi^+\pi^-\gamma$	$0.52\text{–}130\times10^{-6}$	7.4×10^{-2}	7.4×10^{-1}
$\phi \to \pi^0\rho^0 \to \pi^+\pi^-\gamma(\gamma)$	4.3×10^{-2}	7.2×10^{-3}	$<3\times10^{-6}$
$\phi \to \pi^\pm\rho^\mp \to \pi^+\pi^-\gamma(\gamma)$	8.6×10^{-2}	1.7×10^{-3}	$<3\times10^{-6}$
$\phi \to \pi^+\pi^-\pi^0 \to \pi^+\pi^-\gamma(\gamma)$	1.9×10^{-2}	1.3×10^{-3}	$<3\times10^{-6}$

In this decay again CUSB suffers from lack of hermeticity, as well as lack of momentum information. Thus, the dominant background comes from the $\pi\rho$ final states, which give $\pi^+\pi^-\pi^0$ where one of the photons escape the detector. We cannot use energy-momentum constraints and select by mass cuts the signal due to a real ρ being produced. The complete KLOE simulation is still in progress.[14] However, because of

KLOE's hermeticity, and the fact that one measures the charged particles' momenta, applying kinematical constraints and cuts around the ρ mass make background processes (1), (2) and (3) practically negligible despite their larger BR's. The KLOE column in tables IIa and IIb are obtained by using KLOE's geometry and assuming 0.45% momentum resolution. The fractional accuracy achievable has been increased by a factor two, to roughly account for various uncertainties not yet fully evaluated. Similar results were reported by the CMD2 Detector[8] which is also supposed to be hermetic. While its momentum resolution and energy resolution are a factor of two worse than KLOE's, for this signal this is not important because of the width of the f_0. So, in conclusion, if these were the only backgrounds, using general purpose detectors, the photon contamination from the background in the signal region disappears, and one could expect a very good BR determination over the whole range of signal and background BR examined.

Table IIb. Fractional error in BR($\phi \to f_0\gamma$) using only backgrounds with one lost γ

BR($\phi \to f_0\gamma$)	δ(BR)/BR CUSB	δ(BR)/BR KLOE	δ(BR)/BR CMD2
1.0×10^{-6}	3.95	0.033	0.037
1.0×10^{-5}	0.37	0.008	0.008
2.5×10^{-4}	0.016	0.001	0.002

However, we shall see in the next sections that other backgrounds (notably from initial and final state radiation) are by far dominant. Since the misidentified ϕ decay background already essentially disqualifies CUSB for this process, we will present the rest of our simulations in the detector KLOE.[15]

3.2.2 Backgrounds from $e^+e^- \to \mu^+\mu^-\gamma$

The cross section at 1020 MeV for $e^+e^- \to \mu^+\mu^-\gamma$, where the photon energy is between 10 and 120 MeV, is 4.8 nb, equivalent to a BR of 1×10^{-3}, orders of magnitude larger than the signal from $f_0 \to \pi^+\pi^-\gamma$ whose BR is at most 1.3×10^{-4}.[16] The large background contribution from $e^+e^- \to \mu^+\mu^-\gamma$ can however be fully controlled in KLOE because of its good momentum resolution.

While the calorimeter resolution at low energies is relatively poor, events with two charged particles and a photon are four times overconstrained. For ϕ production at rest, momentum conservation gives $E_\gamma = |\mathbf{p}^+ + \mathbf{p}^-|$. From energy conservation, assuming that the positive and negative particles are pions, we get $E'_\gamma = M_\phi - E^+ - E^-$. For $\phi \to \pi^+\pi^-\gamma$ we expect $E_\gamma = E'_\gamma$, while for $e^+e^- \to \mu^+\mu^-\gamma$, the two energies differ by about 17.5

MeV, having used the pion mass for the muons. We have generated by Monte Carlo (MC) simulations the difference $\Delta E_\gamma = E_\gamma - E'_\gamma$, using the expected KLOE momentum resolution.[6] For $\phi \to \pi^+\pi^-\gamma$ decays we find that the rms spread of ΔE_γ is 2 MeV and for $e^+e^- \to \mu^+\mu^-\gamma$, ΔE_γ=17.5 MeV, also with a spread of 2 MeV. Therefore, a cut at in ΔE_γ at 8 MeV gives us a rejection factor of ~2400 against the muon background, which in fact makes it negligible with respect to any other processes with pions in the final states. Note that we have not used the well measured photon direction (±5 mrad) for additional help.

3.2.3 Backgrounds from $e^+e^- \to \pi^+\pi^-\gamma$

As we have seen in the previous sections, the background from misidentified events can be completely controlled in KLOE if we select f_0 candidates by requiring that only a pair of nearly collinear, oppositely charged tracks and one low energy photon, $20 < E_\gamma < 100$ MeV, are present in the detector; that the visible energy equals W, the total energy, and that $\Delta E_\gamma < 8$ MeV, in order to eliminate the $\mu^+\mu^-\gamma$ background.

In the remainder of this chapter, we discuss the various contributions to the final physical state $\pi^+\pi^-\gamma$ from e^+e^- annihilation at the ϕ peak. Four amplitudes, A_1, A_2, A_{ρ^*} and A_{f_0}, contribute. The corresponding intensities, $|A_1|^2$, $|A_2|^2$ and $|A_{\rho^*}|^2$ are background contributions and the f_0 signal is contained in $|A_{f_0}|^2$ and $2\Re(A_{\rho^*}A^*_{f_0})$, as discussed below.

• $A_1 = A(\phi \to \pi_1\rho^* \to \pi_1\pi_2\gamma)$. This is the amplitude for $\phi \to \pi^+\pi^-\gamma$ via $\pi\rho^*$ with the ρ^* coupling to $\gamma\pi$. ρ^* here stands for an internal line, virtual ρ in the corresponding Feynman amplitude. The Feynman diagram for this process is shown in Fig. 2a. We have already discussed the analogous process for neutral pions in Sec. 3.1. Its contribution to the background is small compared to the other sources, see Fig. 3a. In this figure we have taken A_1 at its theoretically estimated level,[10,11] but we have checked[17] that even if we take it at the experimental upper limit, the changes in our results are negligible. The angular dependence of A_1 is shown in Fig. 12. The interference of this background with other processes is also negligible.

• $A_2 = A(e^+e^- \to \gamma\gamma \to \rho^*\gamma \to \pi^+\pi^-\gamma)$. The Feynman diagram for this process is shown in Fig. 2b. This amplitude from *initial state radiation* is the largest incoherent source of background. However, since, as expected for a radiative process, and seen in Fig. 13, $|A_2|^2$ is peaked very sharply at small angles between the photon and the beam, $\theta_{\gamma,\,\mathrm{beam}}$, we reduce its contribution by a factor of ~7 by a cut $|\cos\theta_{\gamma,\,\mathrm{beam}}| < 0.9$, see

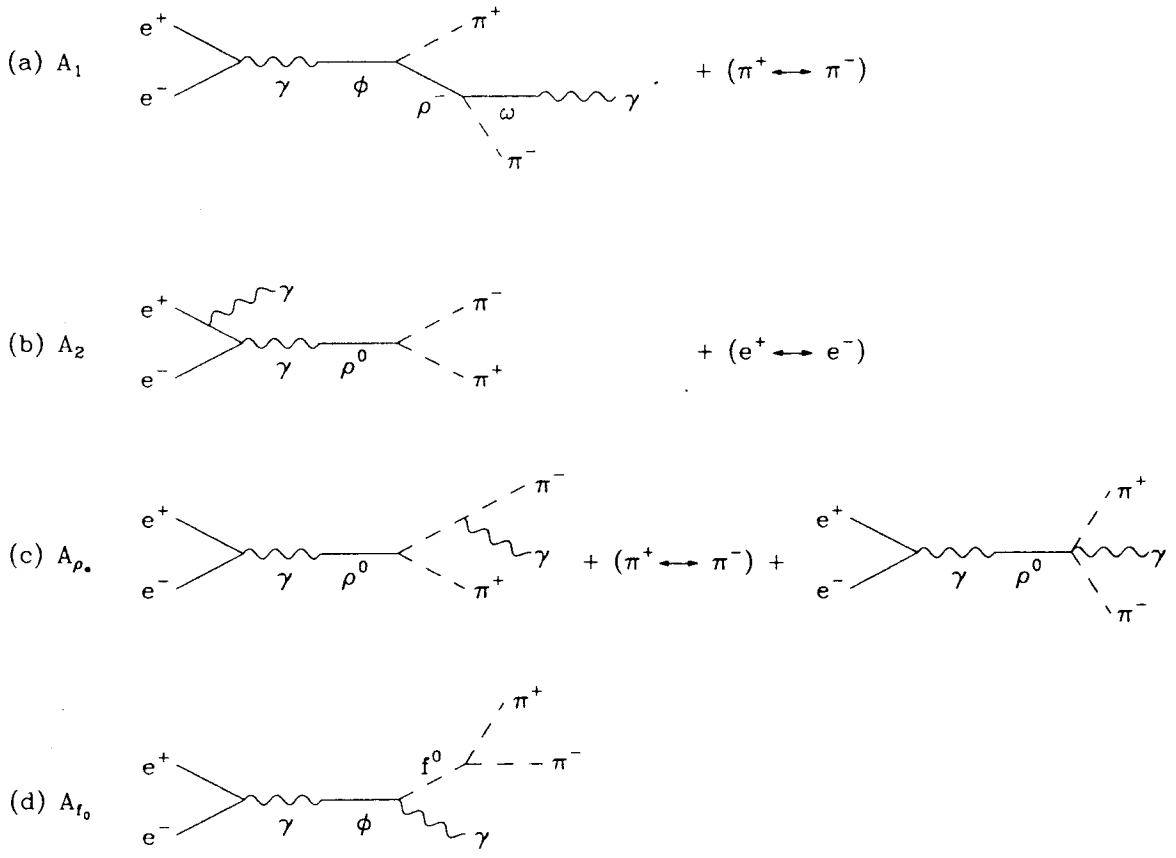

Figure 2. The Feynamn diagrams of the processes discussed in the text.

Fig. 3b.

• $A_{\rho^*} = A(\phi \to \rho^* \to \pi^+\pi^-\gamma)$, the γ being radiated from one of the pions. The Feynman diagram for this process is shown in Fig. 2c. This process contributes approximately one tenth of the A_2 background. However, as expected for a radiative process and seen in Fig. 14, $|A_{\rho^*}|^2$ is peaked at small values of the angle between the pions and the photon in the dipion rest frame, $\theta_{\pi\gamma}$. We therefore restrict $|\cos\theta_{\pi\gamma}|$ to be less than 0.9, see Fig. 3c. The sum of these three sources of background is shown in Fig. 3d, the solid line being without angular cuts, the dashed line with the two angular cuts of $|\cos\theta|$ less than 0.9. With these cuts combined, we retain 80% of the signal and improve the signal to background ratio, S/B, by a factor of $5-6$, see Figs. 8 and 9.

• $|A_{f_0}|^2$ and $2\Re(A_{\rho^*}A^*_{f_0})$. The Feynman diagram for the signal process $\phi \to f_0\gamma$ is shown in Fig. 2d. The angular dependence of $|A_{f_0}|^2$ is $(1 + \cos^2\theta_{\gamma,\ \mathrm{beam}})$, as seen in Fig. 15. The amplitude given in Ref. 5 ignores the bound quark pair wave function of the corresponding mesons, without which the amplitude blows up because of the k^3 factor characteristic of the emission of a photon of momentum k. We damp the amplitude following De Rújula, Georgi and Glashow,[18] with an exponential $Ae^{-x/\Gamma}$,

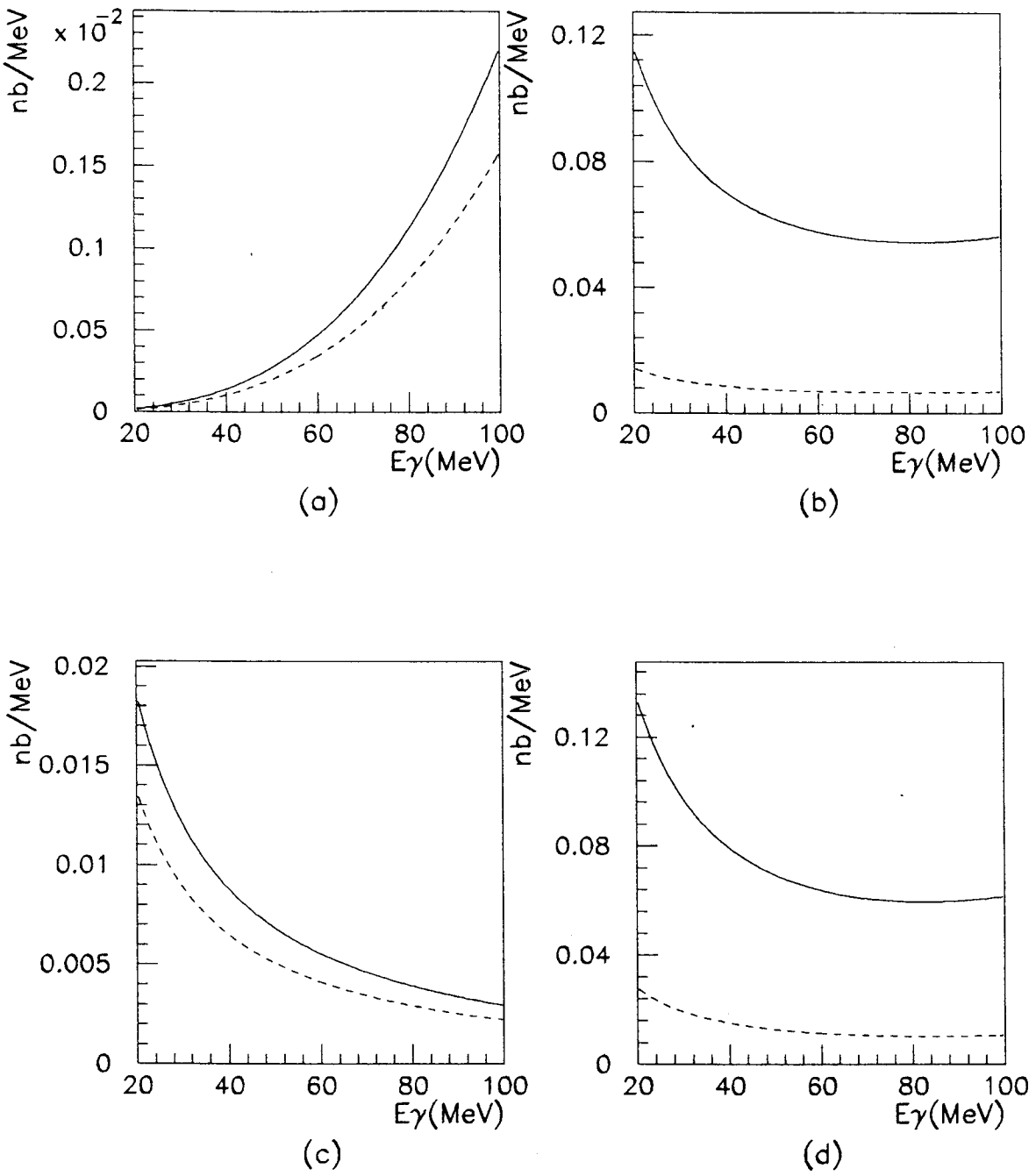

Figure 3. **a.** $|A_1|^2$ contribution; **b.** $|A_2|^2$ contribution; **c.** $|A_{\rho^*}|^2$contribution; **d.** Total incoherent background. Solid lines are without angular cuts, dotted lines are for $|\cos\theta_{\gamma,\ \mathrm{beam}}| < 0.9$ and $|\cos\theta_{\pi\gamma}| < 0.9$.

where $x = s - M^2_{\pi\pi} = 2m_\phi E_\gamma$, Γ=300 MeV, and A=2.65 normalizes the damping factor to 1 at the f_0 peak (42.7 MeV). The signal size depends on $\mathrm{BR}_{\phi f_0\gamma}$. We illustrate it for the two extremes of the range of interest, in Figs. 4a and 5a. We use 52% for $\mathrm{BR}(f_0 \to \pi^+\pi^-)$.

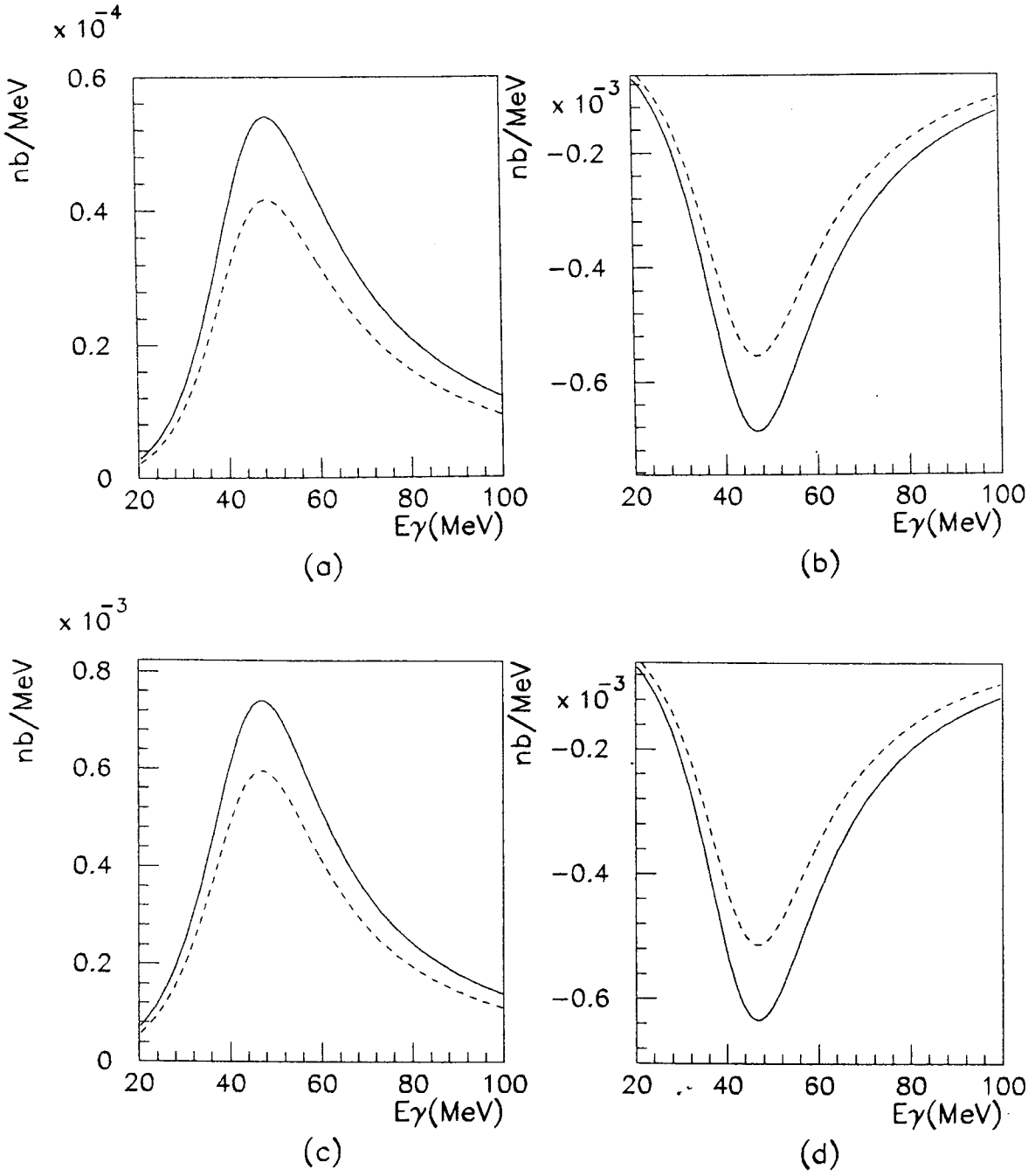

Figure 4. a. γ spectrum: $f_0 \to \pi^+\pi^-\gamma$; **b.** $2\Re(A_\rho \cdot A_{f_0}^*)$; **c.** $|A_{f_0}|^2 - 2\Re(A_\rho \cdot A_{f_0}^*)$; **d.** $|A_{f_0}|^2 + 2\Re(A_\rho \cdot A_{f_0}^*)$. $BR_{\phi f_0 \gamma} = 1 \times 10^{-6}$. Solid lines are without angular cuts, dotted lines are for $|\cos\theta_{\gamma,\,\mathrm{beam}}| < 0.9$ and $|\cos\theta_{\pi\gamma}| < 0.9$.

The interference term $2\Re(A_\rho \cdot A_{f_0}^*)$ is slightly peaked along the beam direction and slightly suppressed along the pions, seen in Fig. 16 in the appendix. Its integrated magnitude is shown for the two extreme cases of the $BR_{\phi f_0 \gamma}$ in Figs. 4b and 5b. For small $BR_{\phi f_0 \gamma}$ the interference term dominates in absolute value over the f_0 term, while the reverse is true for the largest $BR_{\phi f_0 \gamma}$. This interesting cross over is because $|A_{f_0}|^2$ is

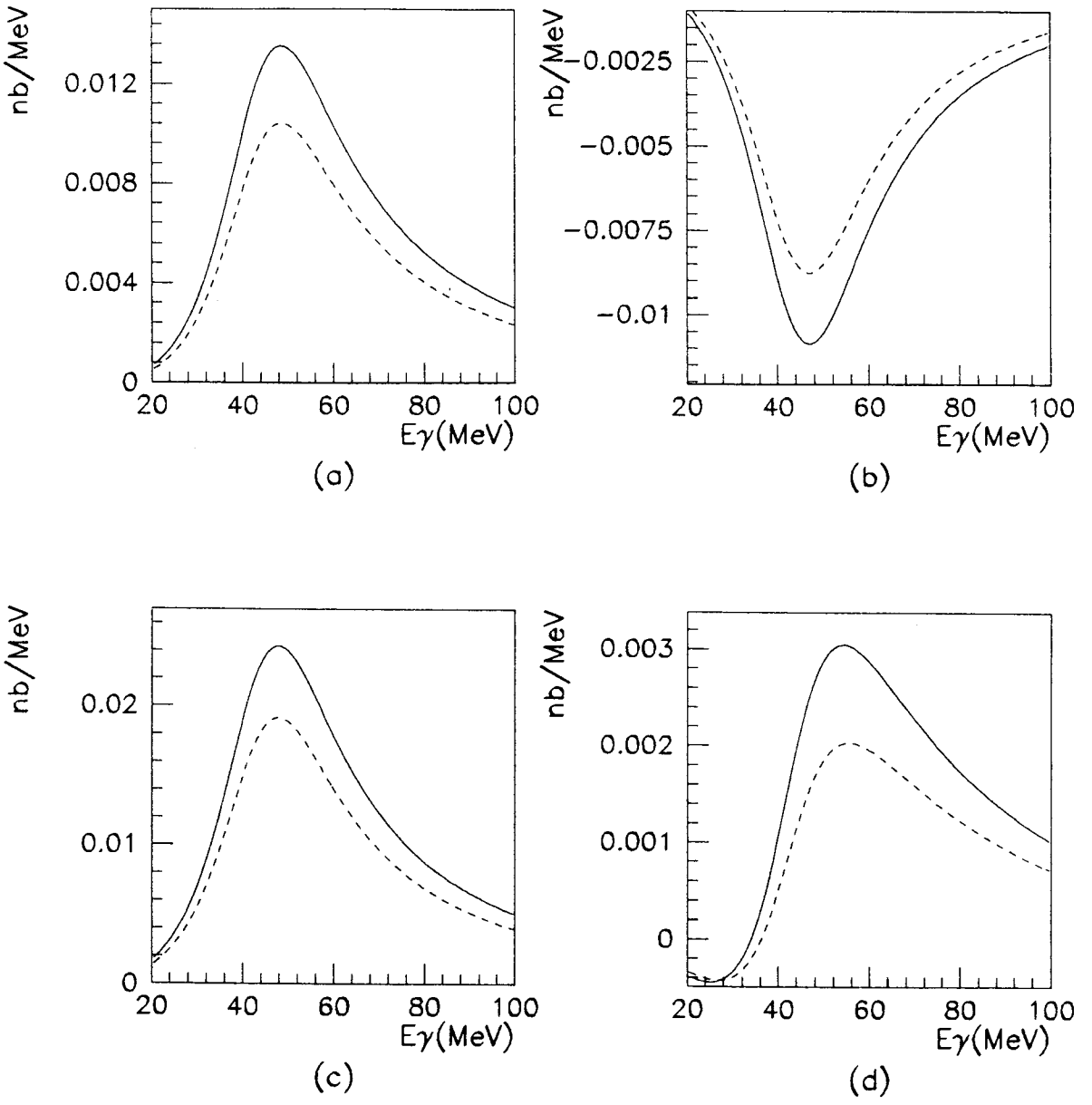

Figure 5. **a.** γ spectrum: $f_0 \to \pi^+\pi^-\gamma$; **b.** $2\Re(A_\rho \cdot A^*_{f_0})$;
c. $|A_{f_0}|^2 - 2\Re(A_\rho \cdot A^*_{f_0})$; **d.** $|A_{f_0}|^2 + 2\Re(A_\rho \cdot A^*_{f_0})$. $\mathrm{BR}_{\phi f_0 \gamma} = 2.5 \times 10^{-4}$. Solid lines are without angular cuts, dotted lines are for $|\cos\theta_{\gamma,\,\mathrm{beam}}| < 0.9$ and $|\cos\theta_{\pi\gamma}| < 0.9$.

proportional to $\mathrm{BR}_{\phi f_0 \gamma}$, whereas the interference term varies as $\sqrt{\mathrm{BR}_{\phi f_0 \gamma}}$. Thus, even for destructive interference, the contribution of $|A_{f_0}|^2 + 2\Re(A_\rho \cdot A^*_{f_0})$ to the total cross section is not always negative. Figs. 4c,d and 5c,d show $|A_{f_0}|^2 \pm 2\Re(A_\rho \cdot A^*_{f_0})$ for the two extremes of the range of interest. For $\mathrm{BR}_{\phi f_0 \gamma} \sim 1.75 \times 10^{-4}$, the integrated contribution to the $\pi^+\pi^-\gamma$ cross section vanishes; however, a dip appears at low γ energies and an

enhancement at high γ energies, allowing detection of the f_0 signal.

The angular dependence of $|A_{f_0}|^2+2\Re(A_{\rho^*}A^*_{f_0})$ also depends on the relative strength of each term, of course reflecting that of the dominant one. To illustrate the complexity of the situation, we chose $\mathrm{BR}_{\phi f_0\gamma}=1.5\times10^{-4}$, where the two terms have about equal strength, and show $\mathrm{d}^2\sigma/\mathrm{d}E_\gamma\mathrm{d}\cos\theta_{\gamma,beam}$ vs E_γ, $\cos\theta_{\gamma,beam}$, and $\mathrm{d}^2\sigma/\mathrm{d}E_\gamma\mathrm{d}\cos\theta_{\pi\gamma}$ vs E_γ, $\cos\theta_{\pi\gamma}$ for constructive interference in Figs. 6a and b respectively. The same quantities in the case of destructive interference are shown in Figs. 7a and b respectively, where dips and enhancements are clearly visible. We also note that the relative strength of $|A_{f_0}|^2$ and $2\Re(A_{\rho^*}A^*_{f_0})$ are modulated by the γ–π angle, upon which A_{ρ^*} depends strongly.

For $\mathrm{BR}_{\phi f_0\gamma}=1\times10^{-6}$, the signal over the background cannot be shown directly. In order to demonstrate the effectiveness of the cuts we show the signal to background (S/B) ratio for the two cases of constructive and destructive interference, Figs. 8a,b. Note that in both cases we enhanced this ratio by about a factor of five, for a net effect of a few %, for either destructive or constructive interference. With the expected DAΦNE luminosity the signal is quite measurable. In Figs. 8c,d we show the S/B for $\mathrm{BR}_{\phi f_0\gamma}=2.5\times10^{-4}$. The signal is certainly much larger and should be much easier to measure.

Fig. 9 shows the MC simulated photon spectrum which would be observed in KLOE (after cuts) for $\phi\to f_0\gamma\to\pi^+\pi^-\gamma$ for the two cases, constructive and destructive interference, for $\mathrm{BR}_{\phi f_0\gamma}=2.5\times10^{-4}$ and assuming $5\times10^{+9}$ ϕ's are produced in the first year of DAΦNE's operations. The incoherent background contribution is also shown. In Fig. 10 we show the resultant estimate of the fractional accuracy that KLOE can achieve in one year's running at DAΦNE, which gives pleasant reassurance that even at the smallest $\mathrm{BR}_{\phi f_0\gamma}$ considered and with destructive interference, the fractional accuracy in the measurement of BR is ten percent. In addition we note that the differential rate $\mathrm{d}^3\Gamma/\mathrm{d}E_\gamma\mathrm{d}\cos\theta_{\gamma,beam}\mathrm{d}\cos\theta_{\pi\gamma}$ clearly contains more information than the integrated cross section, thus it is possible to improve on the results presented. The study of $\phi\to f_0\gamma\to\pi^0\pi^0\gamma$ provides an independent measure of the strength of the $\phi f_0\gamma$ coupling and therefore a check on the determination of its sign in the $\pi^+\pi^-$case, thus completing the picture of the f_0.

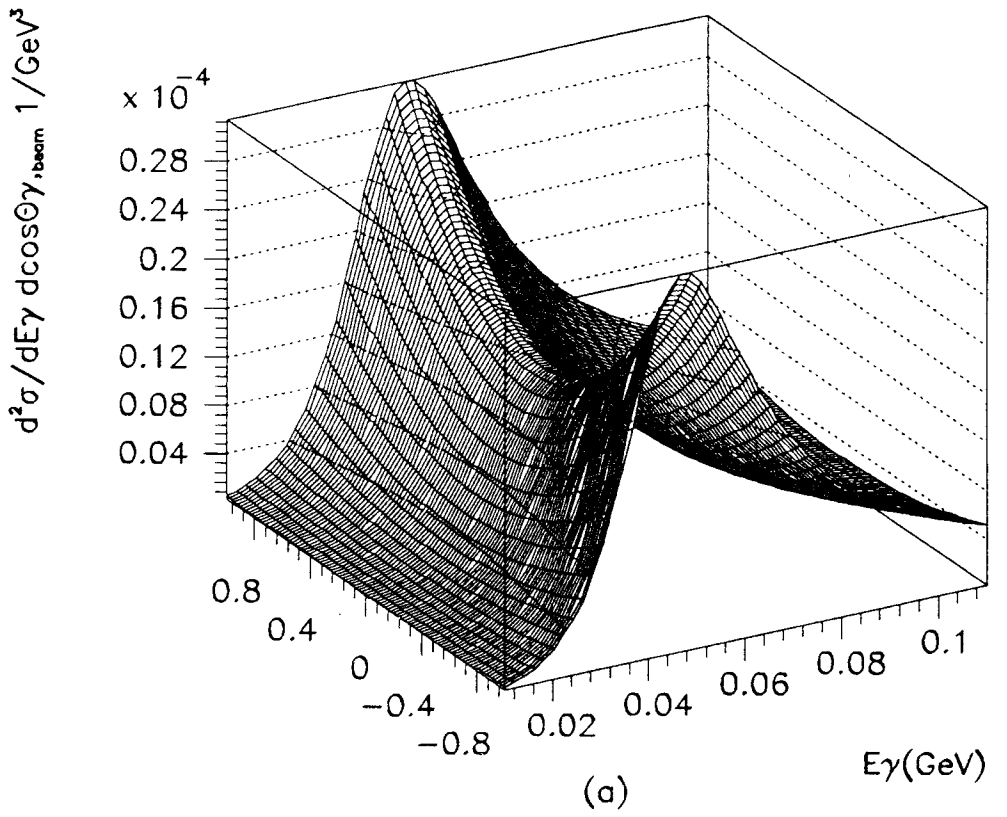

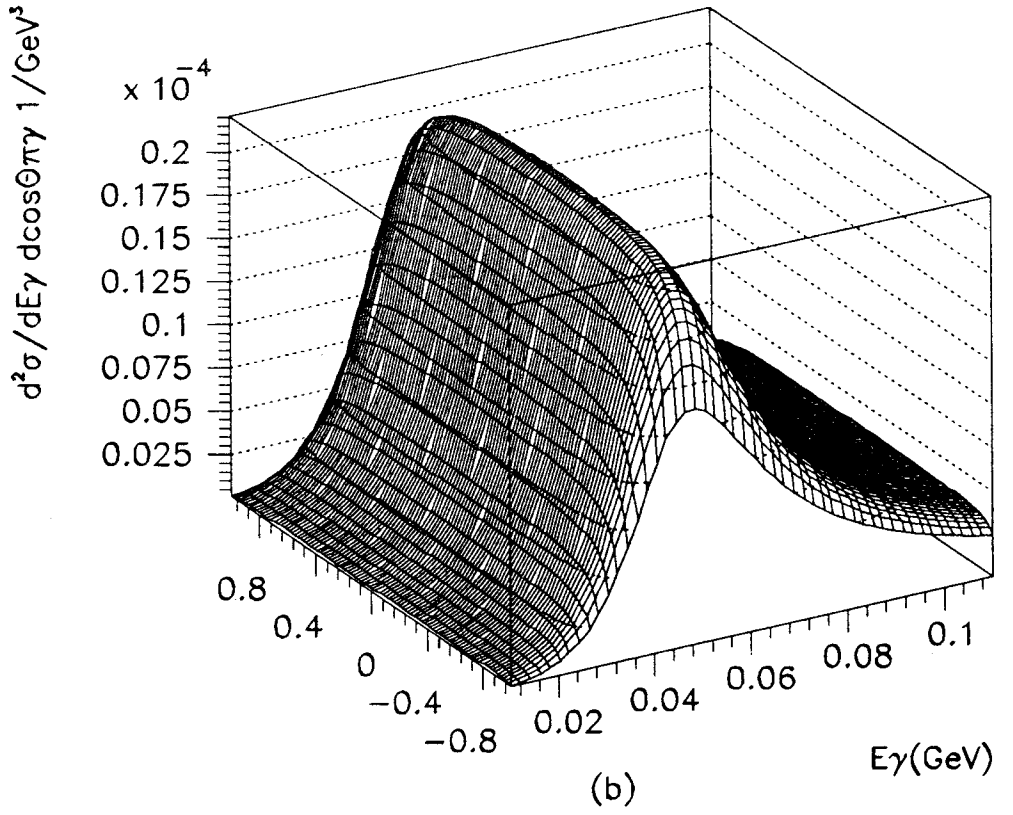

Figure 6. **a.** $d^2\sigma/dE_\gamma d\cos\theta_{\gamma,beam}$ *vs* E_γ, $\cos\theta_{\gamma,beam}$; **b.** $d^2\sigma/dE_\gamma d\cos\theta_{\pi\gamma}$ *vs* E_γ, $\cos\theta_{\pi\gamma}$ for constructive interference, BR=1.5×10^{-4}

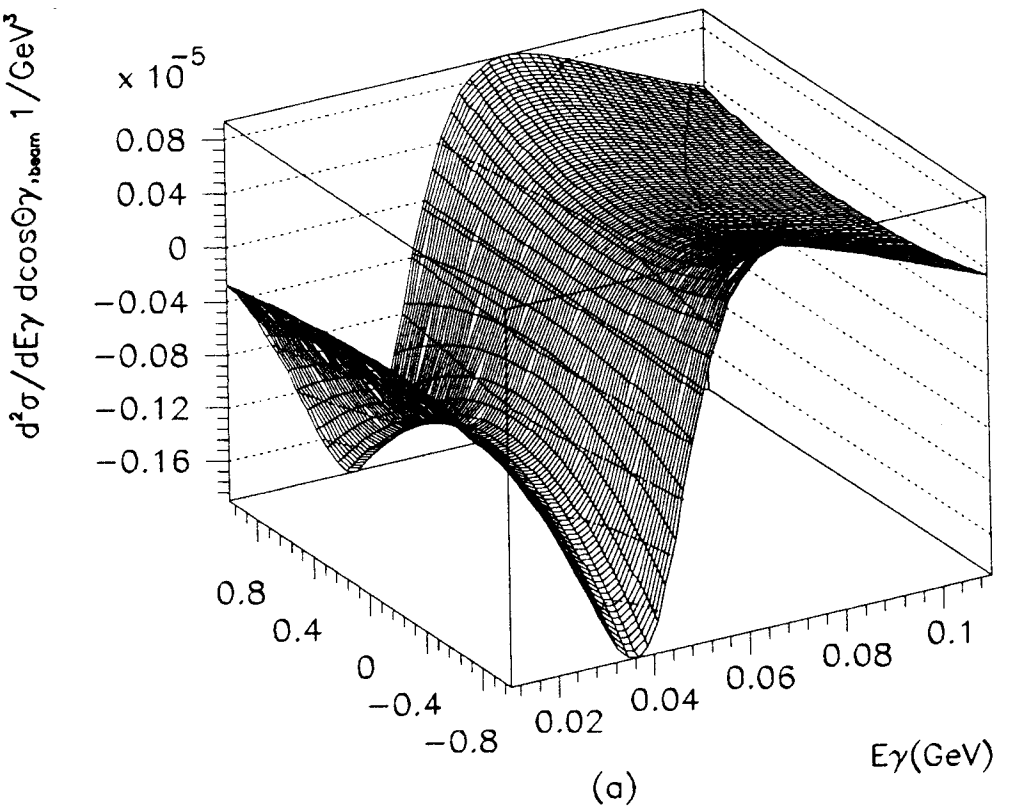

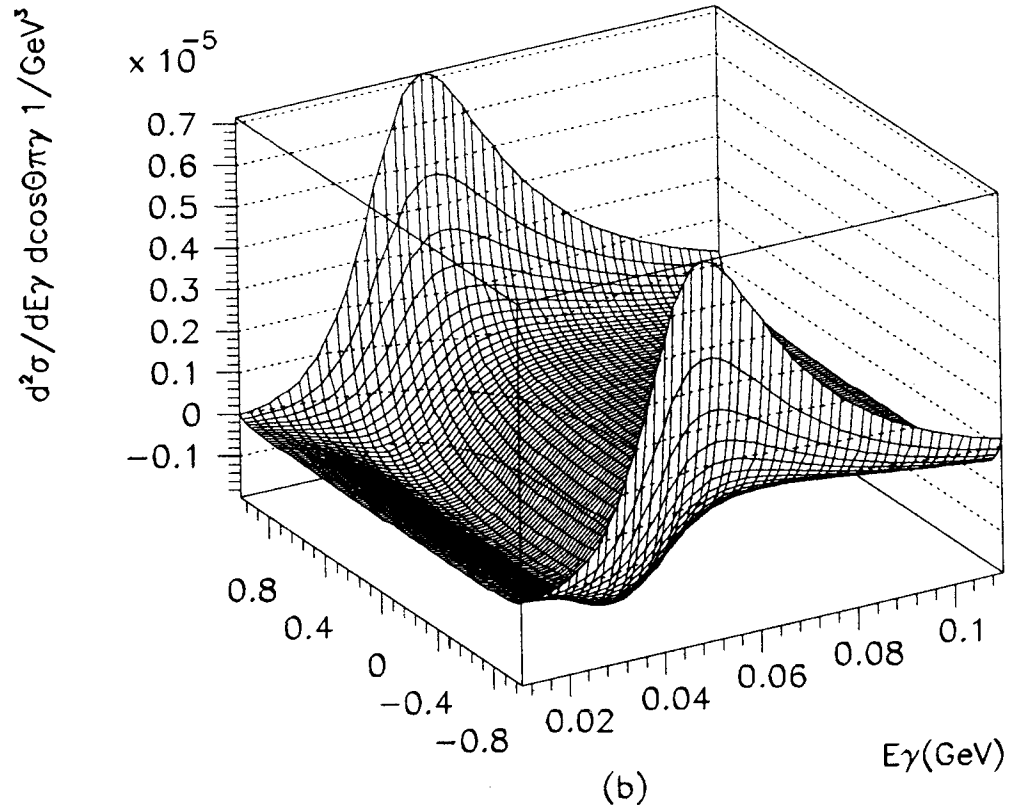

Figure 7. **a.** $\mathrm{d}^2\sigma/\mathrm{d}E_\gamma \mathrm{d}\cos\theta_{\gamma,beam}$ *vs* E_γ, $\cos\theta_{\gamma,beam}$; **b.** $\mathrm{d}^2\sigma/\mathrm{d}E_\gamma \mathrm{d}\cos\theta_{\pi\gamma}$ *vs* E_γ, $\cos\theta_{\pi\gamma}$ for destructive interference, BR=1.5×10^{-4}

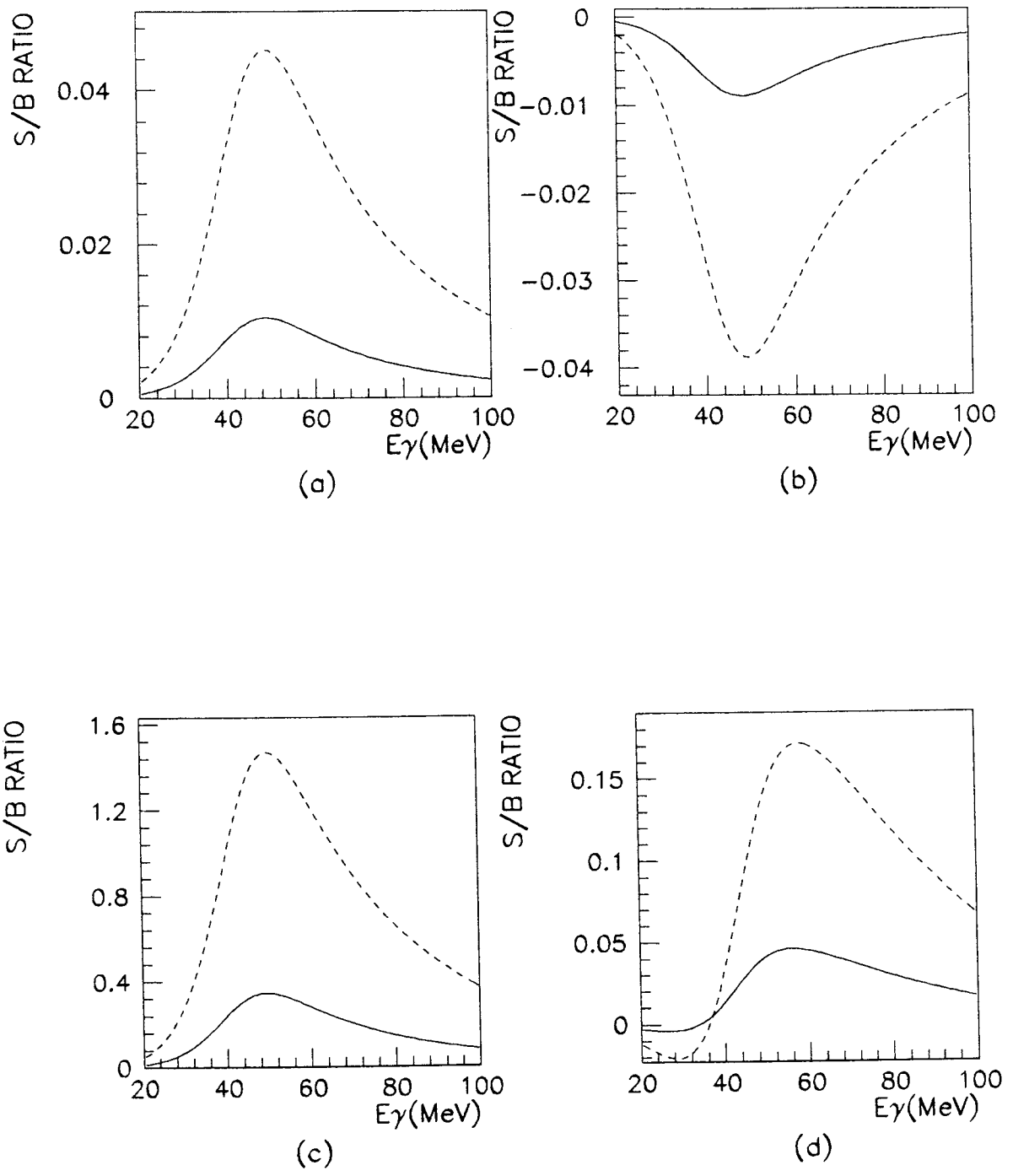

Figure 8. S/B ratio for **a.** constructive **b.** destructive interference, BR=1×10^{-6}; **c.** constructive **d.** destructive interference, BR=2.5×10^{-4}. Solid lines are without angular cuts, dotted lines are for $|\cos\theta_{\gamma,\ \mathrm{beam}}| < 0.9$ and $|\cos\theta_{\pi\gamma}| < 0.9$.

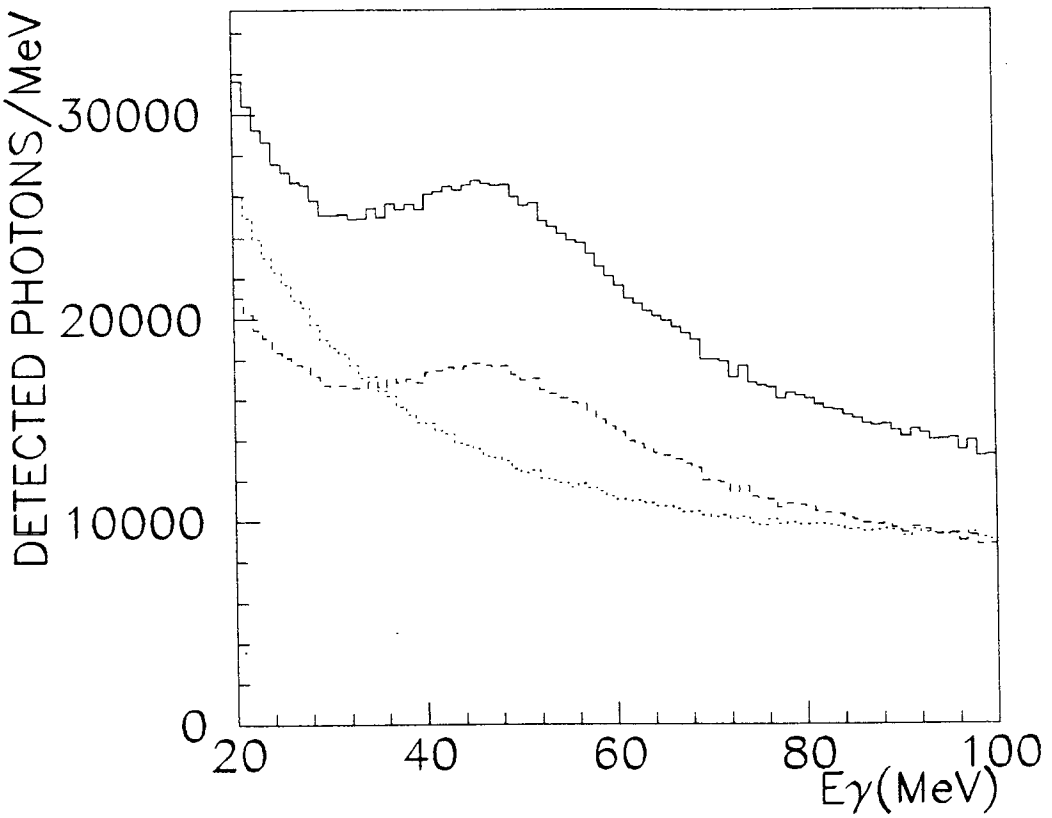

Figure 9. γ spectrum in KLOE from $\phi \to \pi^+\pi^-\gamma$ for BR=2.5×10^{-4} , $5\times10^9\phi$'s (after cuts). Solid and dashed lines are signal + background, constructive and destructive respectively; dotted line is incoherent background alone.

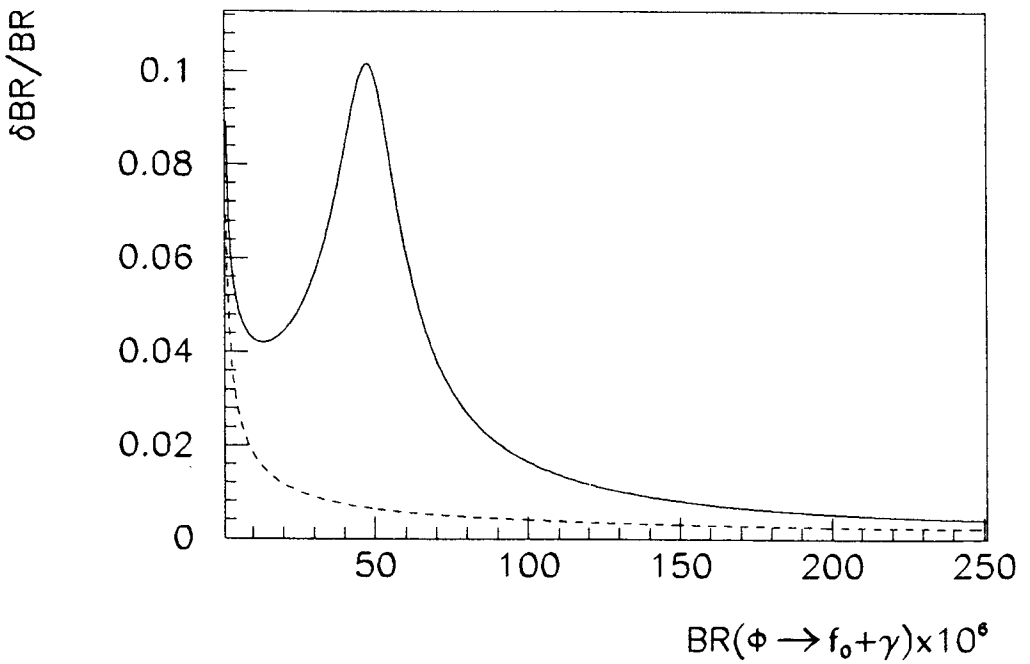

Figure 10. Fractional error on $BR_{\phi f_0\gamma}$ *vs* $BR_{\phi f_0\gamma}$. Solid line is for destructive interference, dashed line for constructive interference.

4. $\phi \to \eta'\gamma$

We have also studied the accuracy achievable by KLOE in the measurement of BR($\phi \to \eta'\gamma$), for an equal running period. This ϕ decay mode has never been seen; the experimental upper limit is 4.1×10^{-4}. Measurement of the BR of this mode will shed light on the gluonium content, $Z_{\eta'}$, of the η'.[19] The rate for radiative decays of the ϕ to pseudoscalar mesons containing $\bar{s}s$ pairs is proportional to the amplitude, Y, of the $\bar{s}s$ component of their wave function, giving the scaling law:

$$\frac{\Gamma(\phi \to \eta'\gamma)}{\Gamma(\phi \to \eta\gamma)} = \left(\frac{Y_{\eta'}}{Y_\eta}\right)^2 \left(\frac{k_{\eta'}}{k_\eta}\right)^3 \sim 4.6 \times 10^{-3} \left(\frac{Y_{\eta'}}{Y_\eta}\right)^2. \tag{4.1}$$

To give an idea of the expected order of magnitude of the branching ratio, for $Z_{\eta'} = 0$ and the $\eta - \eta'$ mixing angle $\theta_p = -20°$,[20] BR($\phi \to \eta'\gamma$) $\sim 1.2 \times 10^{-4}$.

The signature for $\phi \to \eta'\gamma$, $\eta' \to \eta\pi^+\pi^-$ and $\eta \to \gamma\gamma$ is: a pair of charged pions, two photons whose invariant mass equals that of the η, and one low energy photon. The invariant mass of all particles must equal the ϕ mass. By applying these criteria, the efficiency×acceptance for the signal in KLOE is 74.5%. The possible background events are from:

1. $\phi \to \eta\gamma$, BR=$(1.28 \pm 0.06) \times 10^{-2}$, $\eta \to \pi^+\pi^-\pi^0$, product BR 3.0×10^{-3}. Use of kinematical constraints pushes the background down so that the efficiency×acceptance for this background in KLOE is 2.6×10^{-3}.
2. $\phi \to \omega\gamma$, BR<5%, $\omega \to 3\pi$, product BR=4.4×10^{-2}. After kinematical constraints, one finds an efficiency×acceptance for this background in KLOE of 5.9×10^{-3}.
3. $\phi \to \pi^0\rho^0 \to \pi^0\pi^+\pi^-\gamma$, product BR=$(4.8 \pm 0.6) \times 10^{-3}$. Overall kinematical constraints again result in an efficiency×acceptance for this background in KLOE of 5.6×10^{-3}.

We can calculate in this way the fractional accuracy achievable in KLOE for the measurement of this BR. The results are tabulated in table III. In Fig. 11 we show the resultant γ spectrum in KLOE. We note that in the first year's run, KLOE can measure BR's of ~1% of the value in eq. 4.1, for zero gluon content.

Table III. Fractional error in BR($\phi \to \eta'\gamma$) for KLOE.

BR($\phi \to \eta'\gamma$)	δ(BR)/BR
1.0×10^{-5}	0.0634
4.1×10^{-4}	0.0025

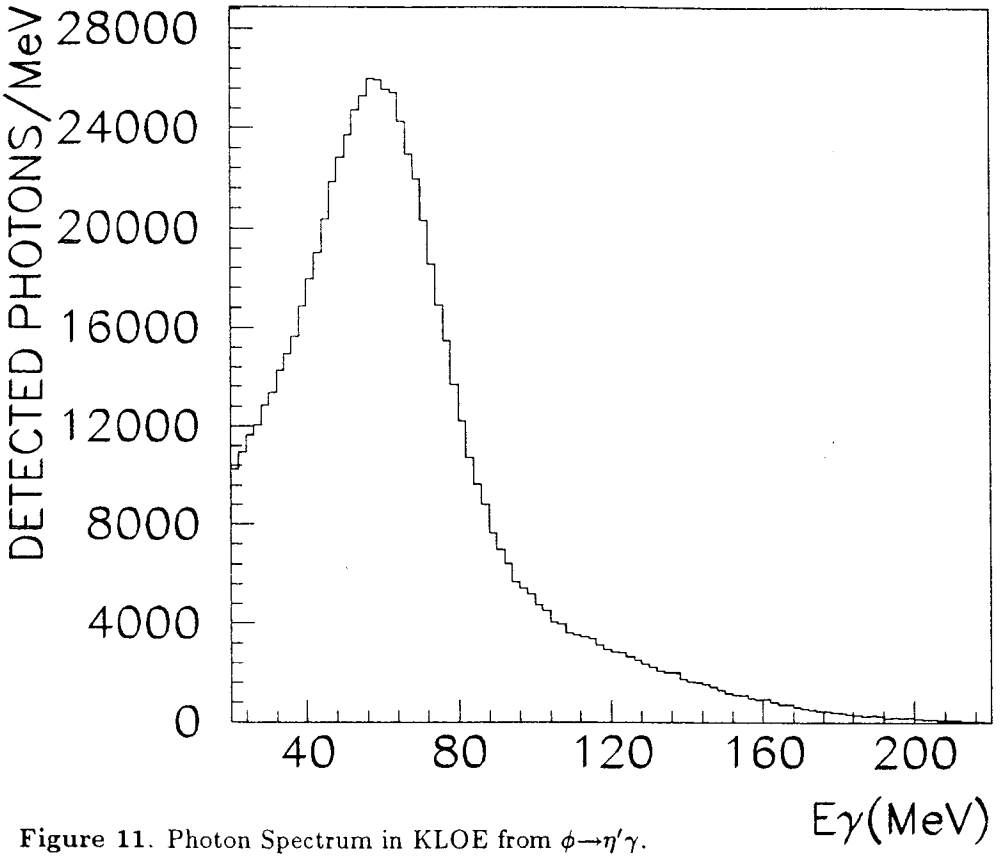

Figure 11. Photon Spectrum in KLOE from $\phi \rightarrow \eta'\gamma$.

5. CONCLUSION

We have studied the experimental problems associated with measuring ϕ radiative decays by choosing two typical and interesting ones: $\phi \rightarrow f_0\gamma$, where the f_0 decays to two neutral pions or two charged pions, and $\phi \rightarrow \eta'\gamma$. We simulated the signal and the expected background in a neutral particle spectrometer: CUSB-II found the decay to neutral pions easily measurable in one year's running time ($\sim 5 \times 10^9$ f's). We also made estimates for the case of two general purpose detectors: KLOE and CMD2, and found the hermeticity of these detectors render the measurements almost trivial. However, the charged pion mode is subject to further background that can only be controlled in a hermetic detector. We found that despite possible destructive interference between the signal and final state radiation, and a large incoherent background from initial state radiation, by using the charged pions, KLOE will be able to determine the sign of the interference, and the magnitude of $BR_{\phi f_0\gamma}$ to accuracies ranging from a fraction of a percent to at most 10 percent in the worst case. The study of $\phi \rightarrow f_0\gamma \rightarrow \pi^0\pi^0\gamma$ provides an independent measure of the strength of the $\phi f_0\gamma$ coupling and therefore a check on the determination of its sign in the $\pi^+\pi^-$case, thus completing the picture

of the f_0. We found the η' search using KLOE relatively easy. Implementation of both types of detectors at DAΦNE is highly desirable and promises to produce good physics.

6. APPENDIX

For completeness, in this Appendix we give the full angular distributions of the ϕ decay to $\pi\pi\gamma$ through a virtual ρ, in other words, the matrix element resulting from calculating the Feynman diagrams starting with e^+e^- rather than with a resonance in an averaged polarization state. This yields the same integrated rates as found previously (Bramon, Grau, and Pancheri[11]) but, in addition, the correct angular distributions, which are necessary for Monte Carlo simulations of these processes.

In general, the full angular dependence of a ϕ decay process, where the ϕ originates in an e^+e^- collision, can be derived by replacing the ϕ polarization vector ϵ^*_μ, in an amplitude given for ϕ decay, by $\bar{e}\gamma_\mu e$, or, if

$$A(\phi \to XYZ) = \epsilon^{*\mu} R_\mu \tag{6.1}$$

we have

$$|\mathcal{A}(e^+e^- \to \phi \to XYZ)|^2_{e^+e^- \text{ spin avg.}} = \left(p^\mu p'^\nu + p'^\mu p^\nu - g^{\mu\nu} p \cdot p'\right) R_\mu R_\nu \tag{6.2}$$

where p and p' are the electron and positron 4-momenta. Thus, the decay width of a ϕ originating in e^+e^- collisions is:

$$\mathrm{d}\Gamma(\phi_{e^+e^-} \to XYZ) = \mathrm{d}\sigma(e^+e^- \to \phi \to XYZ) \frac{\Gamma(\phi \to \text{everything})}{\sigma_{\text{prod}}(e^+e^- \to \phi)} = \frac{\mathcal{K}|\mathcal{A}|^2}{M_\phi^2}, \tag{6.3}$$

where $\mathcal{K}$ is the usual kinematic factor for decays,

$$\mathcal{K} = \frac{1}{64\pi^3} \frac{1}{M_\phi^2} \mathrm{d}E_1 \mathrm{d}E_2 \frac{\mathrm{d}\phi_1}{2\pi} \frac{\mathrm{d}\cos\theta_1}{2} \frac{\mathrm{d}\phi_2}{2\pi} \tag{6.4}$$

with an extra factor of 1/2 if there are two identical particles in the final state. The point of this notation is to isolate the changes needed to go from previous calculations to ones taking into account the ϕ polarization when produced in e^+e^- collision. These are simply: changing from eq. (6.1) to (6.2); the factor of $\frac{1}{M_\phi^2}$ in eq. (6.3), and the missing polarization averaging factor of $\frac{1}{3}$ in eq. (6.4).

We then have, for $\phi \to \rho\pi \to \pi^+\pi^-\gamma$

$$R_\mu = \left(\frac{\epsilon G^2 e}{3g\sqrt{2}}\right) \frac{\epsilon_{\mu\alpha\beta\gamma}(q_\alpha + p^+_\alpha) q^*_\beta \epsilon_{\gamma\delta\epsilon\rho} q_\delta (q_\epsilon + p^+_\epsilon) \epsilon_\rho}{M_\rho^2 - (q + p^+)^2 - iM_\rho\Gamma_\rho} + (p^+ \leftrightarrow p^-) \tag{6.5}$$

where $G = (3\sqrt{2}g^2)/(4\pi^2 f_\pi)$, f_π is the pion decay constant, 132 MeV, g=4.2, and $\epsilon = -0.059$ (see Ref. 11 for further details).

The most compact way to display our result, then, is to borrow the notation of Creutz and Einhorn,[4] correcting a factor of 1/2 and some signs that we find ourselves in disagreement with (we have subsequently confirmed with the authors that these differences were previously unnoticed typographical errors in their published paper):

$$
\begin{aligned}
|\mathcal{A}|^2 = \left(\frac{\epsilon G^2 e}{3g\sqrt{2}}\right)^2 s^2 \Bigg[& \frac{1}{2}|H_1|^2\beta_\pi^2 t \sin^2\theta_\gamma \sin^2\theta_{\pi\gamma} + \frac{1}{2}|H_2|^2\beta_\pi^4 t \sin^2\theta_{\pi\gamma} \\
& \times \left(\cos^2\theta_{\pi\gamma} + \frac{t}{s}\sin^2\theta_{\pi\gamma} - (\cos\theta_\gamma\cos\theta_{\pi\gamma} - \sqrt{\frac{t}{s}}\sin\theta_\gamma\sin\theta_{\pi\gamma}\cos\phi)^2\right) \\
& + |H_3|^2(1+\cos^2\theta_\gamma)/(2s) \\
& + \mathrm{Re}(H_1H_2^*)\beta_\pi^3 t \sin\theta_\gamma \sin^2\theta_{\pi\gamma}\left(\sqrt{\frac{t}{s}}\sin\theta_{\pi\gamma}\cos\theta_\gamma\cos\phi + \sin\theta_\gamma\cos\theta_{\pi\gamma}\right) \\
& + \mathrm{Re}(H_1H_3^*)\beta_\pi\sqrt{\frac{t}{s}}\sin\theta_\gamma\cos\theta_\gamma\sin\theta_{\pi\gamma}\cos\phi + \mathrm{Re}(H_2H_3^*)\beta_\pi^2\sqrt{\frac{t}{s}}\sin\theta_{\pi\gamma} \\
& \times \left(\sin\theta_\gamma\cos\theta_\gamma\cos\theta_{\pi\gamma}\cos\phi + \sqrt{\frac{t}{s}}\sin\theta_{\pi\gamma}(1-\sin^2\theta_\gamma\cos^2\phi)\right)\Bigg].
\end{aligned}
\tag{6.6}
$$

where t is the four-momentum squared of the dipion system, s of the dilepton system, and β_π the velocity of the pions in the dipion rest frame, $\beta_\pi = \sqrt{1-\xi/(1-x)}$. ϕ is the angle between the $e^+e^-\gamma$ plane and the $\pi^+\pi^-$ plane in the lab frame or the dipion rest frame; θ_γ is the photon-beam angle in the lab frame, and $\theta_{\pi\gamma}$ is the angle between the pions and the photon *in the dipion rest frame* related to the pion energy E_π in the lab frame by

$$
y = 1 - \frac{x}{2}\left(1 + \cos\theta_{\pi\gamma}\sqrt{1-\frac{\xi}{1-x}}\right). \tag{6.7}
$$

where $x = 2E_\gamma/\sqrt{s}$, $y = 2E_\pi/\sqrt{s}$, and $\xi = 4m_\pi^2/s$. E_γ and E_π are the energies of the photon and one of the pions in the lab frame. The H_i are general form factors which in our case are given by

$$
H_i = \frac{h_i}{M_\rho^2 + 2M_\phi E_\pi - M_\phi^2 - m_\pi^2 - iM_\rho\Gamma_\rho} + (\pi^+ \leftrightarrow \pi^-) \tag{6.8}
$$

with

$$
h_1 = -\frac{sx}{8}, h_2 = \frac{sx}{8}, h_3 = \frac{s^2}{8}(2x^2 + x\xi - 2x - 2y^2 + 2y). \tag{6.9}
$$

The h_i and $h_i(\pi^+ \leftrightarrow \pi^-)$ come from the direct and crossed diagrams, and the separate contributions from these diagrams and their interference may be easily written in terms of the h_i. Combining all these equations then gives the full angular dependence for $\phi_{e^+e^-} \to \pi^+\pi^-\gamma$ via a virtual ρ; $\phi_{e^+e^-} \to \pi^0\pi^0\gamma$ is identical except for the factor of 1/2

in $\mathcal{K}$. The angle ϕ can be trivially integrated over by replacing $\cos^2\phi$ by $\frac{1}{2}$, and $\cos\phi$ by zero (after first expanding the squared expression in the second line of the above equation).

In Fig. 12a,b we show two views of the angular distribution: $d^2\sigma/dE_\gamma d\cos\theta_{\gamma,\mathrm{beam}}$ vs E_γ, $\cos\theta_{\gamma,\mathrm{beam}}$, and $d^2\sigma/dE_\gamma d\cos\theta_{\pi\gamma}$ vs E_γ, $\cos\theta_{\pi\gamma}$ for $\phi_{e^+e^-} \to \rho\pi \to \pi^0\pi^0\gamma$. The angle $\theta_{\pi\gamma}$ used here is the angle between the pions and the photon *in the dipion rest frame.* For the completeness of the DAΦNE handbook we also include the same views for the other processes considered in this paper: in Fig. 13, initial state radiation; in Fig. 14, final state radiation; in Fig. 15, the signal process, $\phi \to \phi_0\gamma \to \pi^+\pi^-\gamma$; and in Fig. 16, the interference between signal and final state radiation.

ACKNOWLEDGEMENTS

We wish to thank Paolo Franzini for discussions and help in preparing this paper.

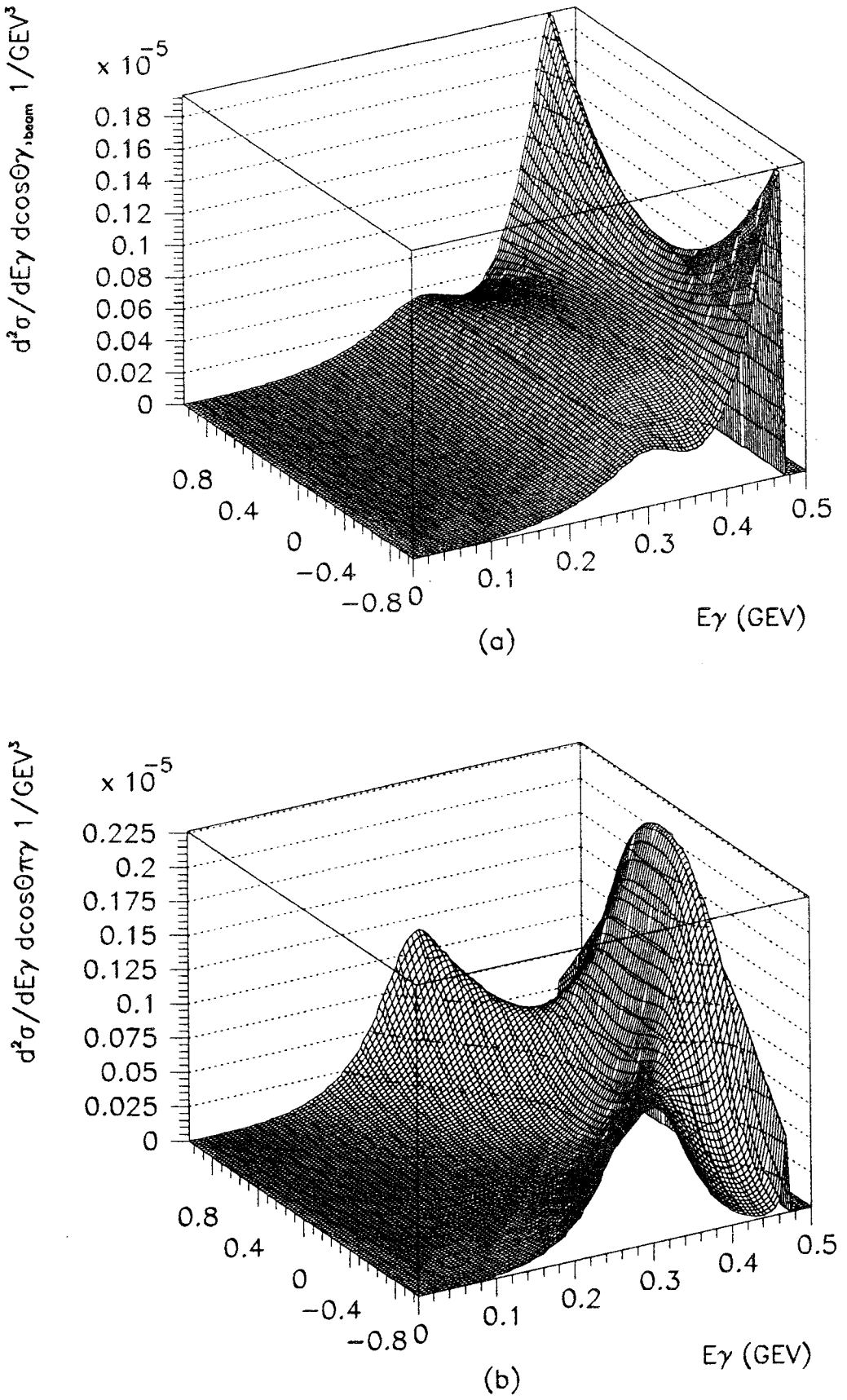

Figure 12. **a.** $d^2\sigma/dE_\gamma d\cos\theta_{\gamma,\mathrm{beam}}$ vs E_γ, $\cos\theta_{\gamma,\mathrm{beam}}$; **b.** $d^2\sigma/dE_\gamma d\cos\theta_{\pi\gamma}$ vs E_γ, $\cos\theta_{\pi\gamma}$ for $\phi_{e^+e^-} \to \rho\pi \to \pi^0\pi^0\gamma$.

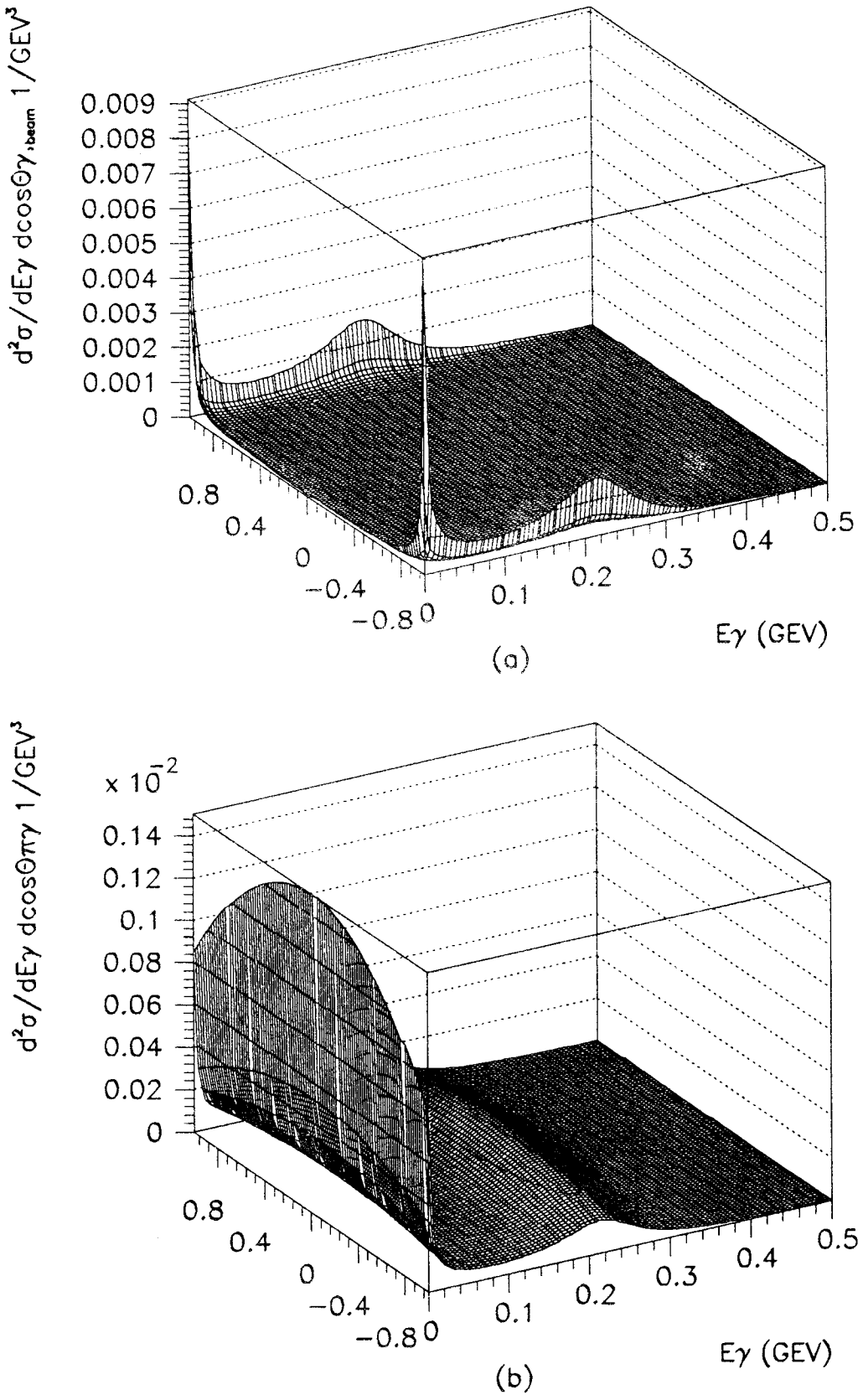

Figure 13. **a.** $d^2\sigma/dE_\gamma d\cos\theta_{\gamma,beam}$ vs E_γ, $\cos\theta_{\gamma,beam}$; **b.** $d^2\sigma/dE_\gamma d\cos\theta_{\pi\gamma}$ vs E_γ, $\cos\theta_{\pi\gamma}$ for initial state radiation.

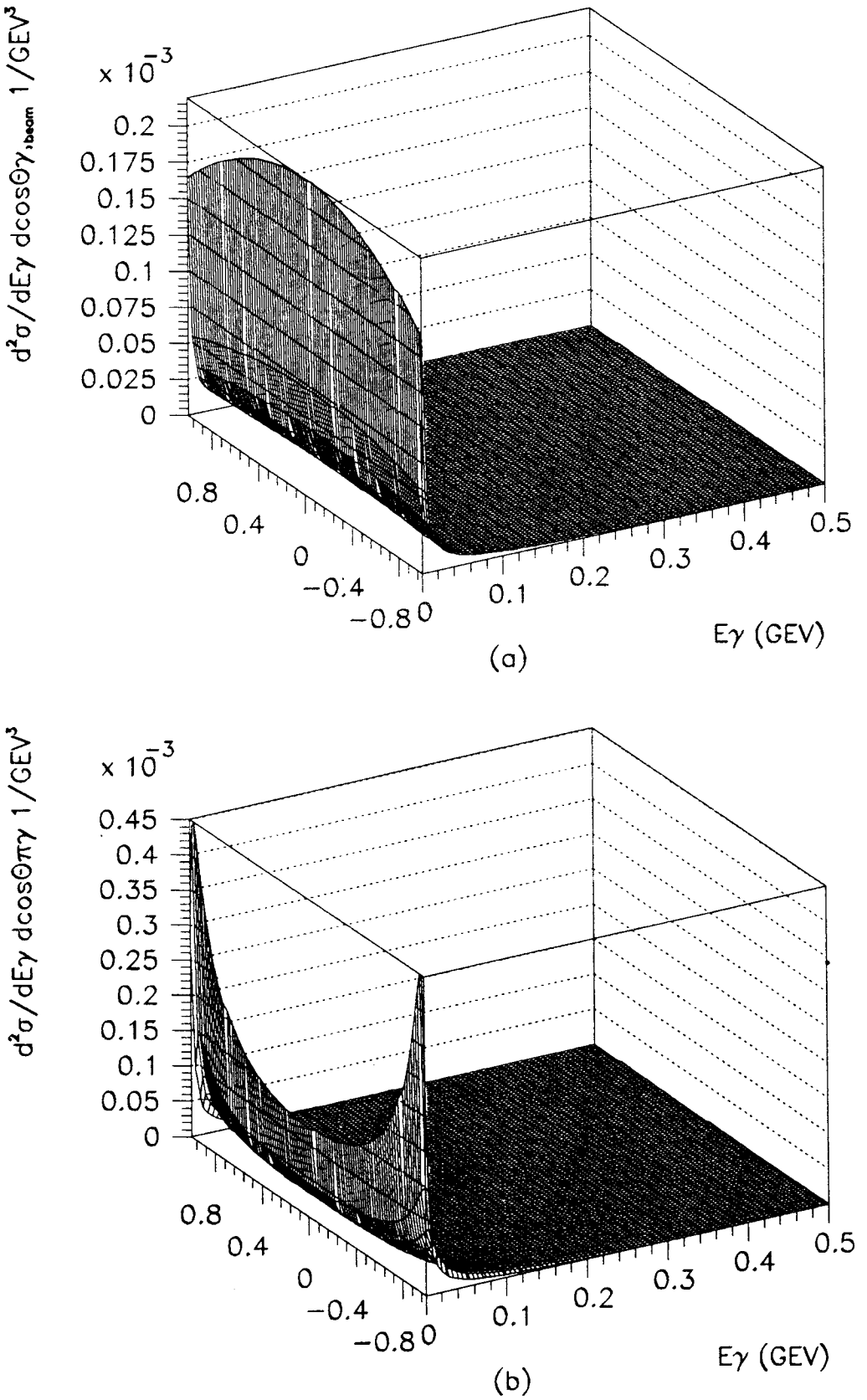

Figure 14. **a.** $d^2\sigma/dE_\gamma d\cos\theta_{\gamma,\mathrm{beam}}$ vs E_γ, $\cos\theta_{\gamma,\mathrm{beam}}$; **b.** $d^2\sigma/dE_\gamma d\cos\theta_{\pi\gamma}$ vs E_γ, $\cos\theta_{\pi\gamma}$ for final state radiation.

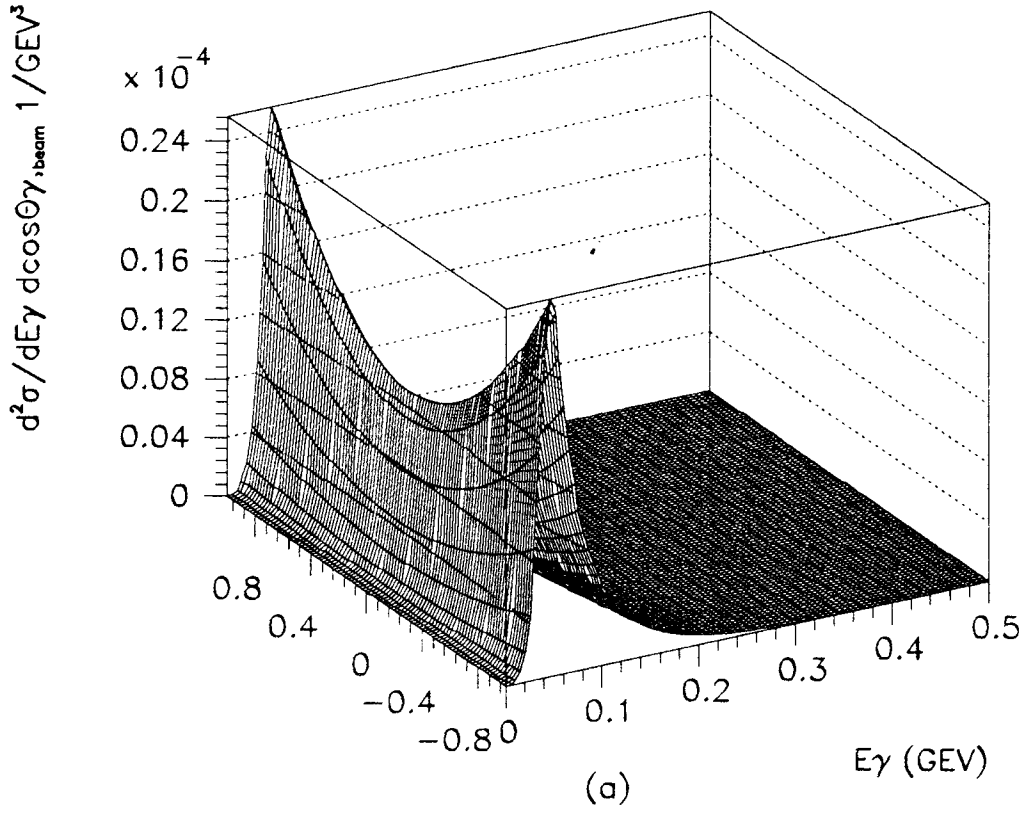

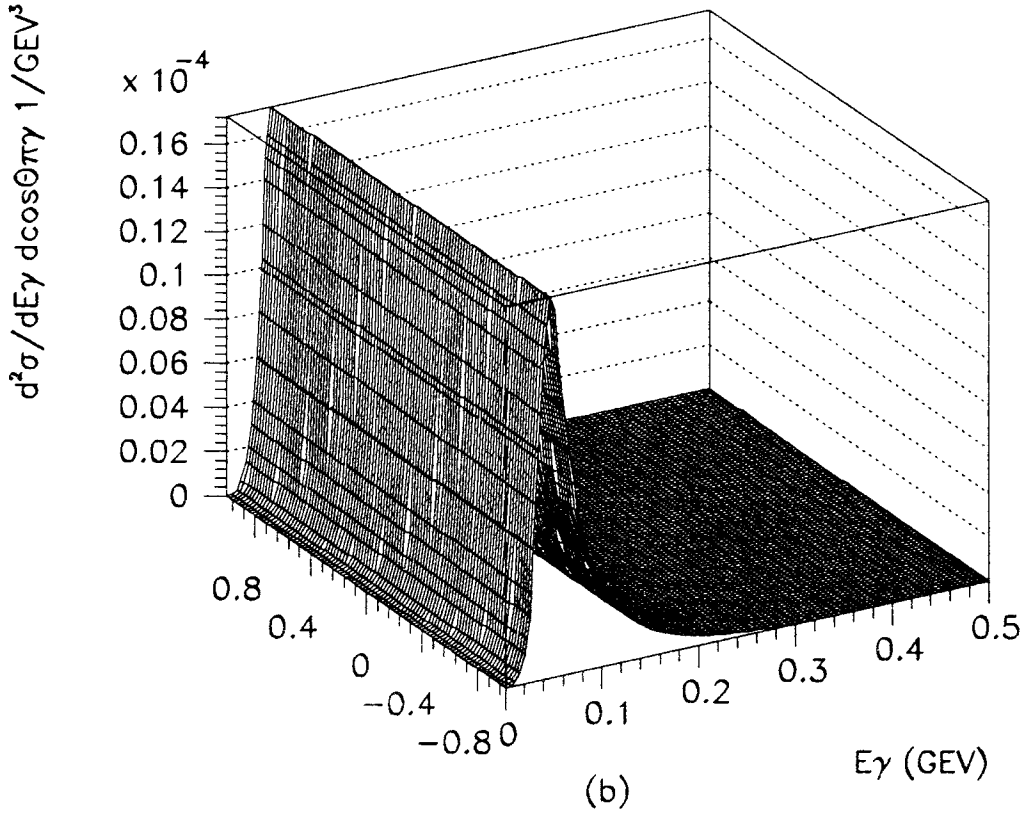

Figure 15. **a.** $d^2\sigma/dE_\gamma d\cos\theta_{\gamma,\mathrm{beam}}$ vs E_γ, $\cos\theta_{\gamma,\mathrm{beam}}$; **b.** $d^2\sigma/dE_\gamma d\cos\theta_{\pi\gamma}$ vs E_γ, $\cos\theta_{\pi\gamma}$ for the signal process, $\phi \to f_0\gamma \to \pi^+\pi^-\gamma$.

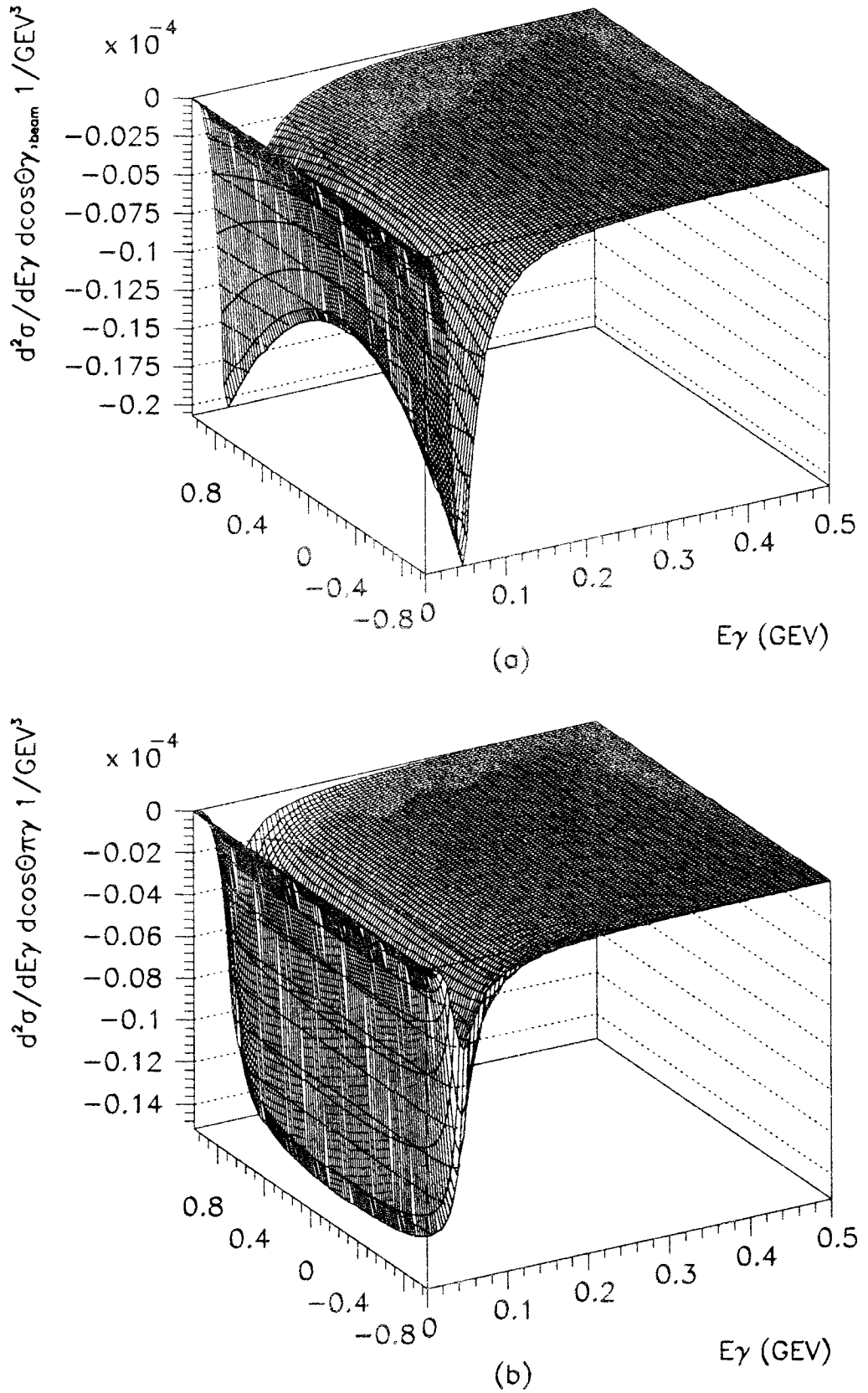

Figure 16. **a.** $d^2\sigma/dE_\gamma d\cos\theta_{\gamma,\mathrm{beam}}$ vs E_γ, $\cos\theta_{\gamma,\mathrm{beam}}$; **b.** $d^2\sigma/dE_\gamma d\cos\theta_{\pi\gamma}$ vs E_γ, $\cos\theta_{\pi\gamma}$ for the interference of final state radiation with the signal process, $\phi \to f_0\gamma \to \pi^+\pi^-\gamma$.

REFERENCES

1. G. Vignola, *Proceedings of the Workshop on Physics and Detectors for Daphne*, G. Pancheri Ed., Frascati, 1991, p. 11.
2. N. Brown and F.E.Close, RAL-91-085.
3. J.J. Hernandez *et al.*, Particle Data Group, Phys. Rev. **B239**, 1 (1990).
4. M. J. Creutz and M. B. Einhorn, Phys. Rev. D1 (1970) 2537.
5. A. Bramon, G. Colangelo, P. J. Franzini, and M. Greco, LNF Preprint LNF-92/022, April 1992.
6. KLOE Proposal, The KLOE Collaboration, LNF Preprint No. 92/019 (IR), April 92.
7. J. Lee-Franzini, Nucl. Instrum. Methods Phys. Res., Sect. **A263**, 35 (1988); P. M. Tuts, Nucl. Instrum. Methods Phys. Res., Sect. **A265**, 243 (1988); R.D. Schamberger et al., Nucl. Instrum. Methods, **A309**, 450 (1991).
8. S. Eidelman, J.A. Thompson and C.H. Yang, *Proceedings of the Workshop on Physics and Detectors for Daphne*, G. Pancheri Ed., LNF dell'INFN, Frascati, 437 (1991).
9. N.N. Achasov *et al.*, Phys. Lett. **96B**, 168 (1980).
10. P. J. Franzini, G. Colangelo, LAPP Preprint ENSLAPP-A-379/92.
11. A. Bramon, A. Grau and G. Pancheri, LNF Preprint LNF-92/011 (P), February 1992.
12. S. Fajfer and R. J. Oakes, Phys. Rev. **D42**, 2392 (1990).
13. Paolo Franzini, LNF Preprint 92/024 (P), April 1992.
14. J. Lee-Franzini, Won Kim, and M. C. Petrucci, KLOE note '92, work in progress.
15. J. Lee-Franzini, Won Kim, and P. J. Franzini, LNF Preprint 92/026(P), April 1992.
16. N.N. Achasov *et al.*, Phys. Lett. **96B**, 168 (1980).
17. J. Lee-Franzini, Won Kim and P. J. Franzini, LNF Preprint 92/025 (P), April 1992.
18. A. De Rújula, H. Georgi, and S. L. Glashow, Phys. Rev. Lett. **37**, 398 (1976).
19. F. Close, *Proceedings of the Workshop on Physics and Detectors for Daphne*, G. Pancheri Ed., Frascati, 1991, p. 309.
20. F. J. Gilman and R. Kauffman, Phys. Rev. **D36**, 2761 (1987); **D37**, 3348 (1988); J. Donoghue, B. R. Holstein and Y.-C. Lin, Phys. Rev. Lett. **55**, 276 (1985).